Neurotrophic factor Neuritin modulates T cell electrical and metabolic state for the balance of tolerance and immunity

Hong Yu[1,2*#], Hiroshi Nishio[1, 2, 3, #], Joseph Barbi[1,2,4, #], Marisa Mitchell-Flack[1,2], Paolo D. A. Vignali[1,2,5], Ying Zheng[1, 2], Andriana Lebid[1,2], Kwang-Yu Chang[1,6], Juan Fu[1,2], Makenzie Higgins[1], Ching-Tai Huang[2, 7], Xuehong Zhang[8], Zhiguang Li[8], Lee Blosser[1], Ada Tam[1], Charles G. Drake[2,9], and Drew M. Pardoll[1,2]

[1] Bloomberg-Kimmel Institute for Cancer Immunotherapy, Immunology and Hematopoiesis Division, Department of Oncology, Johns Hopkins University School of Medicine, Baltimore, Maryland.
[2] The Sidney Kimmel Comprehensive Cancer Center, Johns Hopkins University School of Medicine, Baltimore, Maryland.
[3] Current address: Department of Obstetrics and Gynecology, Keio University School of Medicine, Tokyo 160-8582, Japan
[4] Current address: Department of Immunology, Roswell Park Comprehensive Cancer Center, Buffalo, NY14263, USA
[5] Current address: University of Pittsburgh, Carnegie Mellon.
[6] Current address: National Institute of Cancer Research, National Health Research Institutes, Tainan, Taiwan
[7] Current address: Infectious Diseases, Department of Medicine, Chang Gung Memorial Hospital, Taiwan
[8] Institute of Cancer Stem Cell, Cancer Center, Dalian Medical University, Dalian 116044, China.
[9]Current address: Division of Hematology and Oncology, Herbert Irving Comprehensive Cancer Center, Columbia University Medical Center, New York, New York 10032.
# These authors contributed equally to this work.
*Correspondence to hyu13@jhmi.edu.

Abstract:

The adaptive T cell response is accompanied by continuous rewiring of the T cell's electric and metabolic state. Ion channels and nutrient transporters integrate bioelectric and biochemical signals from the environment, setting cellular electric and metabolic states. Divergent electric and metabolic states contribute to T cell immunity or tolerance. Here, we report that neuritin (Nrn1) contributes to tolerance development by modulating regulatory and effector T cell function. Nrn1 expression in regulatory T cells promotes its expansion and suppression function, while expression in the T effector cell dampens its inflammatory response. Nrn1 deficiency causes dysregulation of ion channel and nutrient transporter expression in Treg and effector T cells, resulting in divergent metabolic outcomes and impacting autoimmune disease progression and recovery. These findings identify a novel immune function of the neurotrophic factor Nrn1 in regulating the T cell metabolic state in a cell context-dependent manner and modulating the outcome of an immune response.

Introduction

Peripheral T cell tolerance is important in restricting autoimmunity and minimizing collateral damage during active immune reactions and is achieved via diverse mechanisms, including T cell anergy, regulatory T (Treg) cell mediated suppression, and effector T (Te) cell exhaustion or deletion (ElTanbouly and Noelle, 2021). Upon activation, Treg and conventional T cells integrate environmental cues and adapt their metabolism to the energetic and biosynthetic demands, leading to tolerance or immunity. Tolerized versus responsive T cells are characterized by differential metabolic states. For example, T cell anergy is associated with reduced glycolysis, whereas activated T effector cells exhibit increased glycolysis (Buck et al., 2017; Geltink et al., 2018; Peng and Li, 2023; Zheng et al., 2009). Cellular metabolic states depend on electrolyte and nutrient uptake from the microenvironment (Chapman and Chi, 2022; Olenchock et al., 2017). Ion channels and nutrient transporters, which can integrate environmental nutrient changes, affect the cellular metabolic choices and impact the T cell functional outcome (Babst, 2020; Bohmwald et al., 2021; Ramirez et al., 2018). Each cell's functional state would correspond with a set of ion channels and nutrient transporters supporting their underlying metabolic requirements. The mechanisms coordinating the ion channel and nutrient transporter expression changes to support the adaptive T cell functional state in the immune response microenvironment remain unclear.

Nrn1, also known as candidate plasticity gene 15 (CPG15), was initially discovered as a neurotrophic factor linked to the neuronal cell membrane through a glycosylphosphatidylinositol (GPI) anchor (Nedivi et al., 1998; Zhou and Zhou, 2014). It is highly conserved across species, with 98% overall homology between the murine and human protein. Nrn1 plays multiple roles in neural development, synaptic plasticity, synaptic maturation, neuronal migration, and survival (Cantallops et al., 2000; Javaherian and Cline, 2005; Nedivi et al., 1998; Putz et al., 2005; Zito et al., 2014). In the immune system, Nrn1 expression has been found in Foxp3^{+} Treg and follicular regulatory T cells (Tfr) (Gonzalez-Figueroa et al., 2021; Vahl et al., 2014), T cells from transplant tolerant recipients (Lim et al., 2013), anergized CD8 cells or CD8 cells from tumor-infiltrating lymphocytes in mouse tumor models (Schietinger et al., 2012; Schietinger et al., 2016; Singer et al., 2016), and in human Treg infiltrating breast cancer tumor tissue (Plitas et al., 2016). Soluble Nrn1 can be released from Tfr cells and act directly on B cells to suppress autoantibody development against tissue-specific antigens (Gonzalez-Figueroa et al., 2021). Despite the observation of Nrn1 expression in Treg cells and T cells from tolerant environments (Gonzalez-

102 Figueroa et al., 2021; Lim et al., 2013; Plitas et al., 2016; Schietinger et al., 2012; Schietinger et
103 al., 2016; Singer et al., 2016), the roles of Nrn1 in T cell tolerance development and Treg cell
104 function have not been explored, and functional mechanism of Nrn1 remains elusive. This study
105 demonstrates that the neurotrophic factor Nrn1 can moderate T cell tolerance and immunity
106 through both Treg and Te cells, impacting Treg cell expansion and suppression while controlling
107 inflammatory response in Te cells.
108
109 **Results**
110 **Nrn1 expression and function in T cell anergy.**
111 To explore the molecular mechanisms underlying peripheral tolerance development, we
112 utilized a system we previously developed to identify tolerance-associated genes (Huang et al.,
113 2004). We compared the gene expression patterns associated with either a T effector/memory
114 response or tolerance induction triggered by the same antigen but under divergent *in vivo*
115 conditions (Huang et al., 2004). Influenza hemagglutinin (HA) antigen-specific TCR transgenic
116 CD4 T cells were adoptively transferred into WT recipients with subsequent HA-Vaccinia virus
117 (VacHA) infection to generate T effector/memory cells while tolerogenic HA-specific CD4s were
118 generated by transfer into hosts with transgenic expression of HA as self-antigen (C3-HA mice,
119 Figure 1A.)(Huang et al., 2004). One of the most differentially expressed genes upregulated in the
120 anergy-inducing condition was Nrn1. Nrn1 expression was significantly higher among cells
121 recovered from C3-HA hosts vs. cells from VacHA infected mice at all time points tested by qRT-
122 PCR (Figure 1A). To further confirm the association of Nrn1 expression with T cell anergy, we
123 assessed Nrn1 expression in naturally occurring anergic polyclonal $CD4^+$ T cells (Ta), which can
124 be identified by surface co-expression of Folate Receptor 4 (FR4) and the ecto-5'-nucleotidase
125 CD73 (Ta, $CD4^+CD44^+FR4^{hi}CD73^{hi}$ cells)(Kalekar et al., 2016). Nrn1 expression was
126 significantly higher in Ta than in naïve CD4 (Tn, $CD4^+CD62L^+CD44^-FR4^-CD73^-$) and antigen-
127 experienced cells (Te, $CD4^+CD44^+FR4^-CD73^-$) under steady-state conditions measured by both
128 qRT-PCR and western blot (Figure 1B). Given that Treg cells, like anergic cells, have roles in
129 maintaining immune tolerance, we queried whether Nrn1 is also expressed in Treg cells. Nrn1
130 expression can be detected in nTreg and induced Treg (iTreg) cells generated *in vitro* (Figure 1C).
131 To evaluate Nrn1 expression under pathological tolerant conditions (Cuenca et al., 2003),
132 we evaluated Nrn1 expression in T cells within the tumor microenvironment. Nrn1 expression in

133 murine Treg cells and non-Treg $CD4^+$ cells from tumor infiltrates were compared to the Treg cells
134 and non-Treg $CD4^+$ T cells isolated from peripheral blood. Nrn1 mRNA level was significantly
135 increased among tumor-associated Treg cells and non-Treg CD4 cells compared to cells from
136 peripheral blood (Figure 1-figure supplement 1A). Consistent with our findings in the mouse tumor
137 setting, the Treg and non-Treg T cells from human breast cancer infiltrates reveal significantly
138 higher Nrn1 expression compared to the peripheral blood Treg and non-Treg cells (Figure 1-figure
139 supplement 1B) (Plitas et al., 2016).

140 $CD4^+$ T cells may pass through an effector stage after activation before reaching an anergic
141 state (Adler et al., 1998; Chen et al., 2004; Huang et al., 2003; Opejin et al., 2020). To evaluate
142 the potential role of Nrn1 expression in T cell tolerance development, we further examined Nrn1
143 expression kinetics after T cell activation. Nrn1 expression was significantly induced after $CD4^+$
144 T cell activation (Figure 1D). Using a Nrn1 specific antibody, Nrn1 can be detected on activated
145 $CD4^+$ and $CD8^+$ cells (Figure 1D, Figure 1-figure supplement 1C). The significant enhancement
146 of Nrn1 expression after T cell activation suggests that Nrn1 may contribute to the process of T
147 cell tolerance development and/or maintenance.

148 To understand the functional implication of Nrn1 expression in immune tolerance, we
149 analyzed Nrn1-deficient ($Nrn1^{-/-}$) mice (Fujino et al., 2011). In the first evaluation of the $Nrn1^{-/-}$
150 colony, $Nrn1^{-/-}$ mice had consistently reduced body weight compared to heterozygous $Nrn1^{+/-}$ and
151 WT ($Nrn1^{+/+}$) mice (Figure 1-figure supplement 2A). The lymphoid tissues of $Nrn1^{-/-}$ mice were
152 comparable to their $Nrn1^{+/-}$ and WT counterparts except for a slight reduction in cell number that
153 was observed in the spleens of $Nrn1^{-/-}$ mice, likely due to their smaller size (Figure 1-figure
154 supplement 2B). Analysis of thymocytes revealed no defect in T cell development (Figure 1-figure
155 supplement 2C), and a flow cytometric survey of the major immune cell populations in the
156 peripheral lymphoid tissue of these mice revealed similar proportions of CD4, CD8 T cells, B cells,
157 monocytes and dendritic cells (DCs) (Figure 1-figure supplement 2D). Similarly, no differences
158 were found between the proportions of anergic and Treg cells in $Nrn1^{-/-}$, $Nrn1^{+/-}$ and WT mice
159 (Figure 1-figure supplement 2E, F), suggesting that Nrn1 deficiency does not significantly affect
160 anergic and Treg cell balance under steady state. Additionally, histopathology assessment of lung,
161 heart, liver, kidney, intestine and spleen harvested from 13 months old $Nrn1^{-/-}$ and $Nrn1^{+/-}$
162 littermates did not reveal any evidence of autoimmunity (data not shown). The comparable level
163 of anergic and Treg cell population among $Nrn1^{-/-}$, $Nrn1^{+/-}$ and WT mice and lack of autoimmunity

164 in Nrn1$^{-/-}$ aged mice suggest that Nrn1 deficiency is not associated with baseline immune
165 abnormalities or overt dysfunction. Due to the similarity between Nrn1$^{+/-}$ and WT mice, we have
166 used either Nrn1$^{+/-}$ or WT mice as our control depending on mice availability and referred to both
167 as "ctrl" in the subsequent discussion.

168 To evaluate the relevance of Nrn1 in CD4^{+} T cell tolerance development, we employed the
169 classic peptide-induced T cell anergy model (Vanasek et al., 2006). Specifically, we crossed OVA
170 antigen-specific TCR transgenic OTII mice onto the Nrn1$^{-/-}$ background. Nrn1$^{-/-}$_OTII^{+} or
171 control_OTII^{+} (ctrl_OTII^{+}) cells marked with Thy1.1^{+} congenic marker (Thy1.1^{+}Thy1.2^{-}), were
172 co-transferred with polyclonal WT Tregs (marked as Thy1.1^{-}thy1.2^{+}), into TCRα knockout mice
173 (TCRα$^{-/-}$), followed by injection of soluble OVA peptide to induce clonal anergy (Figure 1E)
174 (Chappert and Schwartz, 2010; Martinez et al., 2012; Mercadante and Lorenz, 2016; Shin et al.,
175 2014). On day 13 after cell transfer, the proportion and number of OTII cells increased in the Nrn1^{-}
176 $^{/-}$_OTII compared to the ctrl_OTII hosts (Figure 1F). Moreover, Nrn1$^{-/-}$_OTII cells produced
177 increased IL2 than ctrl_OTII upon restimulation (Figure 1G). Anergic CD4 Tconv cells can
178 transdifferentiate into Foxp3^{+} pTreg cells *in vivo* (DL, 2017; Kalekar et al., 2016; Kuczma et al.,
179 2021). Consistent with reduced anergy induction, the proportion of Foxp3^{+} pTreg among Nrn1$^{-/-}$
180 _OTII was significantly reduced (Figure 1H). In parallel with the phenotypic analysis, we
181 compared gene expression between Nrn1$^{-/-}$_OTII and ctrl_OTII cells by RNA Sequencing
182 (RNASeq). Gene set enrichment analysis (GSEA) revealed that the gene set on T cell anergy was
183 enriched in ctrl relative to Nrn1$^{-/-}$_OTII cells (Figure 1I)(Safford et al., 2005). Also, consistent
184 with the decreased transdifferentiation to Foxp3^{+} cells, the Treg signature gene set was
185 prominently reduced in Nrn1$^{-/-}$_OTII cells relative to the ctrl (Figure 1J). Anergic T cells are
186 characterized by inhibition of proliferation and compromised effector cytokines such as IL2
187 production (Choi and Schwartz, 2007). The increased cell expansion and cytokine production in
188 Nrn1$^{-/-}$_OTII cells and the reduced expression of anergic and Treg signature genes all support the
189 notion that Nrn1 is involved in T cell anergy development.

190 Anergic T cells are developed after encountering antigen, passing through a brief effector
191 stage, and reaching an anergic state (Chappert and Schwartz, 2010; Huang et al., 2003; Silva
192 Morales and Mueller, 2018; Zha et al., 2006). Enhanced T cell activation, defective Treg cell
193 conversion or expansion, and heightened T effector cell response may all contribute to defects in
194 T cell anergy induction and/or maintenance (Chappert and Schwartz, 2010; Huang et al., 2003;

195 Kalekar et al., 2016; Silva Morales and Mueller, 2018; Zha et al., 2006). We first examined early
196 T cell activation to understand the underlying cause of defective anergy development in Nrn1$^{-/-}$
197 cells. Nrn1$^{-/-}$ CD4^{+} cells showed reduced T cell activation, as evidenced by reduced CellTrace
198 violet dye (CTV) dilution, activation marker expression, and Ca^{++} entry after TCR stimulation
199 (Figure 1-figure supplement 3A, B, C). The reduced early T cell activation observed in Nrn1$^{-/-}$
200 CD4 cells suggests that the compromised anergy development in Nrn1$^{-/-}$_OTII cells was not caused
201 by enhanced early T cell activation. The defective pTreg generation and/or enhanced effector T
202 cell response may contribute to compromised anergy development.

203 **Compromised Treg expansion and suppression in the absence of Nrn1.**

204 The significant reduction of Foxp3^{+} pTreg among Nrn1$^{-/-}$_OTII cells could be caused by
205 the diminished conversion of Foxp3^{-} Tconv cells to pTreg and/or diminished Treg cell expansion
206 and persistence. To understand the cause of pTreg reduction in Nrn1$^{-/-}$_OTII cells (Figure 1H), we
207 turned to the induced Treg (iTreg) differentiation system to evaluate the capability of Foxp3^{+} Treg
208 development and expansion in Nrn1$^{-/-}$ cells. Similar proportions of Foxp3^{+} cells were observed in
209 Nrn1$^{-/-}$ and ctrl cells under the iTreg culture condition, suggesting that Nrn1 deficiency does not
210 significantly impact Foxp3^{+} cell differentiation. To examine the capacity of iTreg expansion, Nrn1^{-}
211 $^{/-}$ and ctrl iTreg cells were restimulated with anti-CD3, and we found reduced live cells over time
212 in Nrn1$^{-/-}$ iTreg compared to the ctrl (Figure 2A). The reduced live cell number in Nrn1$^{-/-}$ was
213 accompanied by reduced Ki67 expression (Figure 2B). Although Nrn1$^{-/-}$ iTregs retained a higher
214 proportion of Foxp3^{+} cells three days after restimulation, however, when taking into account the
215 total number of live cells, the actual number of live Foxp3^{+} cells was reduced in Nrn1$^{-/-}$ (Figure
216 2C). Treg cells are not stable and are prone to losing Foxp3 expression after extended proliferation
217 (Feng et al., 2014; Floess et al., 2007; Li et al., 2014; Zheng et al., 2010). The increased proportion
218 of Foxp3^{+} cells was consistent with reduced proliferation observed in Nrn1$^{-/-}$ cells. Thus, Nrn1
219 deficiency can lead to reduced iTreg cell proliferation and persistence *in vitro.*

220 The defects observed in iTreg cell expansion *in vitro* prompt further examination of Nrn1^{-}
221 $^{/-}$ nTreg expansion and suppression function *in vivo.* To this end, we tested the suppression capacity
222 of congenically marked (CD45.1^{-}CD45.2^{+}) Nrn1$^{-/-}$ or ctrl nTreg toward CD45.1^{+}CD45.2^{-}
223 responder cells in Rag2$^{-/-}$ mice (Figure 2D). The CD45.1^{+}CD45.2^{-} responder cells devoid of Treg
224 cells were splenocytes derived from Foxp3DTRGFP (FDG) mice pretreated with diphtheria toxin
225 (DT) (Kim et al., 2007; Workman et al., 2011). DT treatment caused the deletion of Treg cells in

226 FDG mice (Kim et al., 2007). Although the CD45.1$^-$CD45.2$^+$ Nrn1$^{-/-}$ and ctrl cell proportions were
227 not significantly different among hosts splenocytes at day 7 post transfer (Figure 2E), Nrn1$^{-/-}$ cells
228 retained a higher Foxp3$^+$ cell proportion and reduced Ki67 expression comparing to the ctrl (Figure
229 2F, G). These findings were similar to our observation of iTreg cells *in vitro* (Figure 2B, C). Nrn1^{-}
230 $^{/-}$ Tregs also showed reduced suppression toward CD45.1$^+$ responder cells, evidenced by increased
231 CD45.1$^+$ proportion and cell number in host splenocytes (Figure 2H).

232 To evaluate the functional implication of Nrn1$^{-/-}$ Treg suppression in disease settings, we
233 challenged the Rag2$^{-/-}$ hosts with the poorly immunogenic B16F10 tumor (Figure 2D). Tumors
234 grew much slower in Nrn1$^{-/-}$ Treg recipients than those reconstituted with ctrl Tregs (Figure 2I).
235 Moreover, the number of CD45.1$^+$ cells in tumor-draining lymph nodes and spleens increased
236 significantly in Nrn1$^{-/-}$ Treg hosts compared to the ctrl group (Figure 2J). Consistently, the
237 CD45.1$^+$ responder cell proportion among tumor lymphocyte infiltrates (TILs) was also increased
238 (Figure 2K), accompanied by an increased proportion of IFNγ$^+$ cells among CD8 TILs from Nrn1^{-}
239 $^{/-}$ Treg hosts (Figure 2L). The increased expansion of CD45.1$^+$ responder cells and reduced tumor
240 growth further confirmed the reduced suppressive capacity of Nrn1$^{-/-}$ Treg cells.

241 **Nrn1 impacts Treg cell electrical and metabolic state**

242 To understand the molecular mechanisms associated with Nrn1$^{-/-}$ Treg cells, we compared
243 gene expression between Nrn1$^{-/-}$ and ctrl iTregs under resting (IL2 only) and activation (aCD3 and
244 IL2) conditions by RNASeq. GSEA on gene ontology database and clustering of enriched gene
245 sets by Cytoscape identified three clusters enriched in resting Nrn1$^{-/-}$ iTreg (Figure 3A, Figure 3-
246 figure supplement Table 1)(Shannon et al., 2003; Subramanian et al., 2005). The "neurotransmitter
247 involved in membrane potential (MP)" and "sodium transport" clusters involved gene sets on the
248 ion transport and cell MP regulation (Figure 3A, Figure 3-figure supplement Table 1). MP is the
249 difference in electric charge between the interior and the exterior of the cell membrane (Abdul
250 Kadir et al., 2018; Blackiston et al., 2009; Ma et al., 2017). Ion channels and transporters for Na$^+$
251 and other ions such as K$^+$, Cl$^-$ *et al.* maintain the ion balance and contribute to cell MP (Blackiston
252 et al., 2009). MP change can impact cell plasma membrane lipid dynamics and affect receptor
253 kinase activity (Zhou et al., 2015). The enrichment of "receptor protein kinase" gene set clusters
254 may reflect changes caused by MP (Figure 3A, Figure 3-figure supplement Table 1). Gene set
255 cluster analysis on activated iTreg cells also revealed the enrichment of the "ion channel and
256 receptor" cluster in Nrn1$^{-/-}$ cells (Figure 3B, Figure 3-figure supplement table 2), supporting the

257 potential role of Nrn1 in modulating ion balances and MP.

258 The "Neurotransmitter receptor activity involved in regulation of postsynaptic membrane
259 potential" gene set was significantly enriched under resting and activation conditions (Figure 3C
260 and D; Figure 3-figure supplement Table 3). The α-amino-3-hydroxy-5-methyl-4-
261 isoxazolepropionic acid receptor (AMPAR) subunits Gria2 and Gria3 are the major components
262 of this gene set and showed increased expression in Nrn1$^{-/-}$ cells (Figure 3D). AMPAR is an
263 ionotropic glutamate receptor that mediates fast excitatory synaptic transmission in neurons. Nrn1
264 has been reported as an accessory protein for AMPAR (Pandya et al., 2018; Schwenk et al., 2012;
265 Subramanian et al., 2019), although the functional implication of Nrn1 as an AMPAR accessory
266 protein remains unclear. The enrichment of MP related gene set prompted the examination of
267 electric status, including MP level and ion channel expressions. We examined the relative MP level
268 by FLIPR MP dye, a lipophilic dye able to cross the plasma membrane, which has been routinely
269 used to measure cell MP changes (Dvorak et al., 2021; Joesch et al., 2008; Nik et al., 2017;
270 Whiteaker et al., 2001). When the cells are depolarized, the dye enters the cells, causing an increase
271 in fluorescence signal. Conversely, cellular hyperpolarization results in dye exit and decreased
272 fluorescence. Compared to ctrl iTreg cells, Nrn1$^{-/-}$ exhibits significant hyperpolarization under
273 both resting and activation conditions (Figure 3E). Consistent with the MP change, the "MF_metal
274 ion transmembrane transporter activity" gene set, which contains 436 ion channel related genes,
275 was significantly enriched and showed a different expression pattern in Nrn1$^{-/-}$ iTregs (Figure 3F;
276 Figure 3-figure supplement 1A and B). The changes in cellular MP and differential expression of
277 ion channel and transporter genes in Nrn1$^{-/-}$ implicate the role of Nrn1 in the balance of electric
278 state in the iTreg cell.

279 MP changes have been associated with changes in amino acid (AA) transporter expression
280 and nutrient acquisition, which in turn influences cellular metabolic and functional state (Yu et al.,
281 2022). To understand whether MP changes in Nrn1$^{-/-}$ are associated with changes in nutrient
282 acquisition and thus the metabolic state, we surveyed AA transport-related gene expression using
283 the "Amino acid transmembrane transporter activity" gene set and found differential AA
284 transporter gene expression between Nrn1$^{-/-}$ and ctrl iTregs (Figure 3G). Electrolytes and AAs
285 entry are critical regulators of mTORC1 activation and T cell metabolism (Liu and Sabatini, 2020;
286 Saravia et al., 2020; Sinclair et al., 2013; Wang et al., 2020). We examined mTORC1 activation
287 at the protein level by evaluating mTOR and S6 phosphorylation via flow cytometry. We found

288 reduced phosphorylation of mTOR and S6 in activated Nrn1$^{-/-}$ iTreg cells (Figure 3H). We further
289 performed a nutrient-sensing assay to evaluate the role of ion and nutrient entry in mTORC1
290 activation. Nrn1$^{-/-}$ and ctrl iTreg cells were starved for one hour in a nutrient-free buffer, followed
291 by adding RPMI medium with complete ions and nutrients, and cultured for two more hours. While
292 adding the medium with nutrients clearly increased the mTOR and S6 phosphorylation, the degree
293 of change was significantly less in Nrn1$^{-/-}$ than in the ctrl (Figure 3I). Consistently, GSEA on
294 Hallmark gene sets reveal reduced gene set enrichment relating to the mTORC1 signaling,
295 corroborating the reduced pmTOR and pS6 detection in Nrn1$^{-/-}$ cells. Moreover, Nrn1$^{-/-}$ cells also
296 showed reduced expression of glycolysis, fatty acid metabolism, and oxidative phosphorylation
297 related gene sets under both resting and activating conditions (Figure 3J, Figure 3-figure
298 supplement 1C), indicating changes in metabolic status. Since previous work has identified
299 mTORC1 to be an important regulator of aerobic glycolysis and given that our GSEA data
300 suggested changes in glycolysis (Figure 3J) (Salmond, 2018), we performed the seahorse assay
301 and confirmed reduced glycolysis among Nrn1$^{-/-}$ cells (Figure 3K). Examination of mitochondrial
302 bioenergetic function revealed a similar oxygen consumption rate (OCR) between Nrn1$^{-/-}$ and ctrl
303 cells (Figure 3K). Thus, Nrn1 expression can affect the iTreg electric state, influence ion channel
304 and nutrient transporter expression, impact nutrient sensing, modulate metabolic state, and
305 contribute to Treg expansion and suppression function.

306 **Nrn1 impact effector T cell inflammatory response.**

307 CD4^{+} T cells can pass through an effector stage on their way to an anergic state (Huang et
308 al., 2003). Since Nrn1 expression is significantly induced after T cell activation (Figure 1D), Nrn1
309 might influence CD4^{+} effector (Te) cell differentiation, affecting anergy development. Nrn1 may
310 exert different electric changes due to distinct ion channel expression contexts in Te cells than in
311 Tregs. We first evaluated Nrn1$^{-/-}$ Te cell differentiation *in vitro.* Nrn1 deficient CD4 Te cells
312 showed increased Ki67 expression, associated with increased cytokine TNFα, IL2, and IFNγ
313 expression upon restimulation (Figure 4A). To evaluate Nrn1$^{-/-}$ Te cell response *in vivo*, we crossed
314 Nrn1$^{-/-}$ with FDG mice and generated Nrn1$^{-/-}$_FDG and ctrl_FDG mice, which enabled the
315 elimination of endogenous Treg cells (Figure 4B). Deleting endogenous Foxp3^{+} Treg cells using
316 DT will cause the activation of self-reactive T cells, leading to an autoimmune response (Kim et
317 al., 2007; Nystrom et al., 2014). Upon administration of DT, we observed accelerated weight loss
318 in Nrn1$^{-/-}$_FDG mice, reflecting enhanced autoimmune inflammation (Figure 4C). Examination of

319 T cell response revealed a significant increase in Ki67 expression and inflammatory cytokine
320 TNFα, IL2, and IFNγ expression among Nrn1$^{-/-}$ CD4 cells on day 6 post DT treatment (Figure 4D),
321 consistent with the findings *in vitro*. The proportion of Foxp3^{+} cells was very low on day 6 post
322 DT treatment and comparable between Nrn1$^{-/-}$ and the ctrl (Figure 4E), suggesting that the
323 differential Te cell response was not due to the impact from Treg cells. Thus, Nrn1 deficiency
324 enhances Te cell response *in vitro* and *in vivo.*

325 To identify molecular changes responsible for Nrn1$^{-/-}$ Te phenotype, we compared gene
326 expression between Nrn1$^{-/-}$ and ctrl Te cells by RNASeq. GSEA and Cytoscape analysis identified
327 a cluster of gene sets on "membrane repolarization", suggesting that Nrn1 may also be involved
328 in the regulation of MP under Te context (Figure 4F, Figure 4-figure supplement Table 4)
329 (Shannon et al., 2003; Subramanian et al., 2005). While the "membrane_repolarization" gene set
330 was enriched in Nrn1$^{-/-}$ (Figure 4G), the "Neurotransmitter receptor activity involved in regulation
331 of postsynaptic membrane potential" gene set was no longer enriched, but the AMPAR subunit
332 Gria3 expression was still elevated in Nrn1$^{-/-}$ Te cells (Figure 4-figure supplement 1A). Although
333 MP in Te cells was comparable between Nrn1$^{-/-}$ and ctrl (Figure 4H), the "MF_metal ion
334 transmembrane transporter activity" gene set was significantly enriched in Nrn1$^{-/-}$ with different
335 gene expression patterns (Figure 4I, Figure 4-figure supplement 1B), indicative of different electric
336 state. The significant enrichment of ion channel related genes in Nrn1$^{-/-}$ Te cells was in line with
337 the finding in Nrn1$^{-/-}$ iTreg cells, supporting the notion that Nrn1 expression may be involved in
338 ion balance and MP modulation.

339 Examination of nutrient transporters revealed that the "Amino acid transmembrane
340 transporter activity" gene set was significantly enriched in Nrn1$^{-/-}$ cells than the ctrl (Figure 4J).
341 Along with the enrichment of ion channel and nutrient transporter genes (Figure 4I and J), we
342 found enhanced mTOR and S6 phosphorylation in Nrn1$^{-/-}$ Te cells (Figure 4K). We also compared
343 nutrient sensing capability between Nrn1$^{-/-}$ and ctrl Te cells, as outlined in Figure 3I. Nrn1$^{-/-}$ Te
344 showed increased mTOR and S6 phosphorylation after sensing ions and nutrients in RPMI medium
345 (Figure 4L), confirming the differential impact of ions and nutrients on Nrn1$^{-/-}$ and ctrl Te cells.
346 GSEA on Hallmark collection showed enrichment of mTORC1 signaling gene set (Figure 4M),
347 corroborating with increased pmTOR and pS6 detection in Nrn1$^{-/-}$ Te cells. Along with increased
348 mTORC1 signaling, Nrn1$^{-/-}$ Te cells also showed enrichment of gene sets on glycolysis and
349 proliferation (Figure 4M). Evaluation of metabolic changes by seahorse confirmed increased

350 glycolysis in Nrn1$^{-/-}$ cells, while the OCR remained comparable between Nrn1$^{-/-}$ and ctrl (Figure
351 4N). These *in vitro* studies on Te cells indicate that Nrn1 deficiency resulted in the dysregulation
352 of the electrolyte and nutrient transport program, impacting Te cell nutrient sensing, metabolic
353 state, and the outcome of inflammatory response.

354 **Nrn1 deficiency exacerbates autoimmune disease**

355 The coordinated reaction of Treg and Te cells contributes to the outcome of the immune
356 response. We employed the experimental autoimmune encephalomyelitis (EAE), the murine
357 model of multiple sclerosis (MS) to evaluate the overall impact of Nrn1 on autoimmune disease
358 development. Upon EAE induction, the incidence and time to EAE onset in Nrn1$^{-/-}$ mice were
359 comparable to the ctrl mice, but the severity, disease persistence, and body weight loss were
360 increased in Nrn1$^{-/-}$ mice (Figure 5A). Exacerbated EAE was associated with significantly
361 increased CD45^{+} cell infiltrates, increased CD4^{+} cell number, increased proportion of MOG-
362 specific CD4 cells, and reduced proportion of Foxp3^{+} CD4 cells in the Nrn1$^{-/-}$ spinal cord (Figure
363 5B-E). Moreover, we also observed increased proportions of IFN□$^{+}$ and IL17^{+} CD4 cells in Nrn1^{-}
364 $^{/-}$ mice (Figure 5F). Thus, the results from EAE corroborated with earlier data and confirmed the
365 important role of Nrn1 in establishing immune tolerance and modulating autoimmunity.
366

367 **Discussion**

368 T cell expansion and functional development depend on adaptive electric and metabolic
369 changes, maintaining electrolyte balances, and appropriate nutrient uptake. The negative charge of
370 the plasma membrane, ion channel expression pattern, and function are key characteristics
371 associated with the cellular electric state in different systems, impacting cell proliferation and
372 function (Blackiston et al., 2009; Emmons-Bell and Hariharan, 2021; Kiefer et al., 1980; Monroe
373 and Cambier, 1983; Sundelacruz et al., 2009). The electrolytes and nutrients, including amino
374 acids, metabolites, and small peptides transported through ion channels and nutrient transporters,
375 are also regulators and signaling agents impacting the choice of cellular metabolic pathways and
376 functional outcomes (Hamill et al., 2020). In this study, we report that the neurotropic factor Nrn1
377 expression influences CD4 T cell MP, ion channels, and nutrient transporter expression patterns,
378 contributing to differential metabolic states in Treg and Te cells. Nrn1 deficiency compromises
379 Treg cell expansion and suppression while enhancing Te cell inflammatory response, exacerbating
380 autoimmune disease.

381 Bioelectric controls have been defined as a type of epigenetics that can control information
382 residing outside of genomic sequence (Levin, 2021). The sum of ion channels and pump activity
383 generates the ionic gradient across the cell membrane, establishing the MP level and bioelectric
384 state. Cells with the same MP can have different ion compositions, and the same ion channel may
385 have a differential impact on MP when in combination with different ion channels (Abdul Kadir
386 et al., 2018). Consistent with this notion, Nrn1 deficiency has differential impacts on the cellular
387 electric state under the Treg and Te cells with different ion channel combinations. Altered MP was
388 detected in Nrn1 deficient Treg cells (Figure 3E), while comparable MP was observed between
389 Nrn1$^{-/-}$ and ctrl Te cells (Figure 4H). The MP level determined by ion channels and pump activity
390 can influence the nutrient transport pattern, establishing a metabolic and functional state matching
391 the MP level (Blackiston et al., 2009; Emmons-Bell and Hariharan, 2021; Kiefer et al., 1980;
392 Monroe and Cambier, 1983; Sundelacruz et al., 2009; Yu et al., 2022). Yu et al. reported that
393 macrophage MP modulates plasma membrane phospholipid dynamics and facilitates cell surface
394 retention of nutrient transporters, thus supporting nutrient uptake and impacting the inflammatory
395 response (Yu et al., 2022). Nutrient transport is key to T cell fate decisions and has been considered
396 signal 4 to T cell fate choices (Chapman and Chi, 2022; Long et al., 2021). The changes in ion
397 channel related gene expression and MP level in Nrn1$^{-/-}$ cells were accompanied by differential
398 expression of AA transporter genes and nutrient sensing activity that impacted mTORC1 pathway
399 activation and cellular glycolytic state (Figures 3 and 4). These results corroborate previous
400 observations on the connection of MP in nutrient acquisition and metabolic change and support
401 the role of Nrn1 in coordinating T cell electric and metabolic adaptation (Yu et al., 2022).
402 Although Nrn1, as a small GPI-anchored protein, does not have channel activity by itself,
403 it has been identified as one of the components in the AMPAR complex (Pandya et al., 2018;
404 Schwenk et al., 2012; Subramanian et al., 2019). Na^+-influx through the AMPA type ionotropic
405 glutamate receptor can quickly depolarize the postsynaptic compartment and potentiate synaptic
406 transmission in neurons. We have observed increased expression of AMPAR subunits in Nrn1$^{-/-}$
407 iTreg and Te cells (Figure 3D, Figure 4-figure supplement 1), implicating potential change in
408 AMPAR activity in Nrn1$^{-/-}$ under Treg and Te cell context. Glutamate secreted by proliferating
409 cells may influence T cell function through AMPAR. High glutamate levels are detected at the
410 autoimmune disease site and tumor interstitial fluid (Bonnet et al., 2020; McNearney et al., 2004;
411 Sullivan et al., 2019). Moreover, AMPAR has been implicated in exacerbating autoimmune

412 disease (Bonnet et al., 2015; Sarchielli et al., 2007). The increased expression of AMPAR subunits
413 in Nrn1$^{-/-}$ cells supports the potential connection of Nrn1 and AMPAR and warrants future
414 investigation on the possibility that Nrn1 functions through AMPAR, impacting T cell electric
415 change. Besides AMPAR, Nrn1 has been reported to function through the insulin receptor and
416 fibroblast growth factor pathway (Shimada et al., 2016; Yao et al., 2012). Subramanian et al have
417 suggested that rather than a traditional ligand with its cognate receptor, Nrn1 may function as an
418 adaptor to receptors to perform diverse cell-type-specific functions (Subramanian et al., 2019).
419 Our results do not rule out these possibilities.
420 Overall, we found that Nrn1 expression in Treg and Te cells can impact cellular electric
421 state, nutrient sensing, and metabolism in a cell context dependent manner. The predominant
422 enrichment of ion channel related gene sets in both Treg and Te cell context underscores the
423 importance of Nrn1 in modulating ion balance and MP. The changes in ion channels and nutrient
424 transporter expression in Treg and Te cells and associated functional consequences highlight the
425 importance of Nrn1 in coordinating cell metabolic changes through channels and transporters
426 during the adaptive response and contribute to the balance of tolerance and immunity.
427
428 **Materials and Methods**
429 **Mouse models.**
430 The Nrn1$^{-/-}$ mice (Fujino et al., 2011), Foxp3DTRGFP (FDG)(Kim et al., 2007), and TCR$\alpha^{-/-}$ mice
431 were obtained from the Jackson Laboratory. OTII mice on Thy1.1^{+} background was kindly
432 provided by Dr. Jonathan Powell. Rag2$^{-/-}$ mice were maintained in our mouse facility. 6.5 TCR
433 transgenic mice specific for HA antigen and C3HA mice (both on the B10.D2 background) have
434 been described previously (Huang et al., 2004). Nrn1$^{-/-}$ mice were crossed with OTII mice to
435 generate Nrn1$^{-/-}$_OTII^{+} mice, ctrl_OTII^{+} mice. Nrn1$^{-/-}$ mice were also crossed with FDG mice to
436 generate Nrn1$^{-/-}$_FDG and ctrl_FDG mice. All mice colonies were maintained in accordance with
437 the guidelines of Johns Hopkins University and the institutional animal care and use committee
438
439 **Antibodies and Reagents.**
440 We have used the following antibodies: Anti-CD3 (17A2), anti-CD4 (RM4-5), anti-CD8a (53-6.7),
441 anti-CD25 (PC61), anti-CD45.1 (A20), anti-CD45.2 (104), anti-CD62L (MEL-14), CD73
442 (TY/111.8), anti-CD90.1 (OX-7), anti-CD90.2 (30-H12), anti-TCR V□□5.1, 5.2 (MR9-4), anti-

443 PD1 (29F.1A12), anti-IFNγ (XMG1.2), anti-IL17α (TC11-18H10.1), anti-TNFα (MP6-XT22),
444 anti-Tbet (4B10), anti-Ki67 (16A8) were purchased from Biolegend. Anti-CD44 (IM7), CD45
445 (30-F11), anti-CD69(H1.2F3) were purchased from BD Bioscience. Anti-FOXP3 (FJK-16s) was
446 purchased from eBioscience. The flow cytometry data were collected using BD Celesta (BD
447 Biosciences) or Attune Flow Cytometers (ThermoFisher). Data were analyzed using FlowJo (Tree
448 Star) software.
449 Mouse monoclonal anti-Nrn1 antibody (Ab) against Nrn1 was custom-made (A&G
450 Pharmaceutical). The specificity of anti-Nrn1 Ab was confirmed by ELISA, cell surface staining
451 of Nrn1 transfected 293T cells, and western blot of Nrn1 recombinant protein and brain protein
452 lysate from WT mice or $Nrn1^{-/-}$ mice (data not shown). $OVA_{323-339}$ peptide and MOG_{35-55} was
453 purchased from GeneScript. Incomplete Freund's adjuvant (IFA) and Mycobacterium tuberculosis
454 H37Ra (killed and desiccated) were purchased from Difco. Pertussis toxin was purchased from
455 List Biological Laboratories and diphtheria toxin was obtained from Millipore-Sigma.
456
457 **Cell purification and culture.**
458 Naïve CD4 cells were isolated from the spleen and peripheral lymph node by a magnetic bead-
459 based purification according to the manufacturer's instruction (Miltenyi Biotech). Purified CD4
460 cells were stimulated with plate-bound anti-CD3 (5ug/ml, Bio-X-Cell) and anti-CD28 (2ug/ml,
461 Bio-X-Cell) for 3 days, in RPMI1640 medium supplemented with 10%FBS, HEPES,
462 penicillin/streptomycin, MEM Non-Essential Amino Acids, and β-mercaptoethanol. For iTreg cell
463 differentiation, cells were stimulated in the presence of human IL2 (100u/ml, PeproTech), human
464 TGFβ (10ng/ml, PeproTech), anti-IL4, and anti-IFNγ antibody (5ug/ml, Clone 11B11 and clone
465 XMG1.2, Bio-X-Cell) in 10% RPMI medium. $CD4^+$ Te cells were differentiated without
466 additional cytokine or antibody for three days, followed by additional culture for 2 days in IL2
467 100u/ml in 10%RPMI medium. nTreg cells were isolated by sorting from the FDG $CD4^+$ fraction
468 based on $Foxp3^+$GFP and CD25 expression ($CD4^+CD25^+GFP^+$). Alternatively, nTreg cells were
469 enriched from CD4 cells by positive selection using the $CD4^+CD25^+$ Regulatory T Cell Isolation
470 Kit from Miltenyi.
471
472 **Self-antigen induced tolerance model.**
473 $1x10^6$ HA-specific $Thy1.1^+$ 6.5 CD4 cells from donor mice on a B10.D2 background were

474 transferred into C3-HA recipient mice, where HA is expressed as self-antigen in the lung; or into
475 WT B10.D2 mice followed by infection with Vac-HA virus ($1x10^6$ pfu). HA-reactive T cells were
476 recovered from the lung-draining lymph node of C3-HA host mice or WT B10.D2 Vac-HA
477 infected mice at indicated time points by cell sorting. RNA from sorted cells was used for qRT-
478 PCR assay examining Nrn1 expression.
479
480 **Peptide-induced T cell anergy model.**
481 $5x10^5$ Polyclonal Treg cells from $CD45.1^+$ C57BL/6 mice were mixed with $5x10^6$ $thy1.1^+$ OTII
482 cells from $Nrn1^{-/-}$_OTII or ctrl_OTII mice and transferred by *i.v.* injection into $TCR\alpha^{-/-}$ mice.
483 100ug of $OVA_{323–339}$ dissolved in PBS was administered *i.v.* on days 1, 4, and 7 after cell transfer.
484 Host mice were harvested on day 13 after cell transfer, and cells from the lymph node and spleen
485 were further analyzed.
486
487 ***In vivo* Treg suppression assay.**
488 nTreg cells from $CD45.2^+CD45.1^-$ $Nrn1^{-/-}$ or ctrl mice ($5x10^5$/mouse) in conjunction with $CD45.1^+$
489 splenocytes ($2x10^6$/mouse) from FDG mice were cotransferred i.p. into $Rag2^{-/-}$ mice. The $CD45.1^+$
490 splenocytes were obtained from FDG mice pretreated with DT for 2 days to deplete Treg cells.
491 Treg suppression toward $CD45.1^+$ responder cells was assessed on day 7 post cell transfer.
492 Alternatively, 7 days after cell transfer, $Rag2^{-/-}$ hosts were challenged with an *i.d.* inoculation of
493 B16F10 cells ($1x10^5$). Tumor growth was monitored daily. Treg-mediated suppression toward
494 anti-tumor response was assessed by harvesting mice day 18-21 post-tumor inoculation.
495
496 **Induction of autoimmunity by transient Treg depletion.**
497 To induce autoimmunity in $Nrn1^{-/-}$_FDG and ctrl_FDG mice, 1ug/mouse of DT was administered
498 i.p. for two consecutive days, and the weight loss of treated mice was observed over time.
499
500 **EAE induction**
501 EAE was induced in mice by subcutaneous injection of 200 μg $MOG_{35–55}$ peptide with 500 μg M.
502 tuberculosis strain H37Ra (Difco) emulsified in incomplete Freund Adjuvant oil in 200ul volume
503 into the flanks at two different sites. In addition, the mice received 400 ng pertussis toxin (PTX;
504 List Biological Laboratories) *i.p.* at the time of immunization and 48 h later. Clinical signs of EAE

505 were assessed daily according to the standard 5-point scale (Miller et al., 2007): normal mouse; 0,
506 no overt signs of disease; 1, limp tail; 2, limp tail plus hindlimb weakness; 3, total hindlimb
507 paralysis; 4, hindlimb paralysis plus 75% of body paralysis (forelimb paralysis/weakness); 5,
508 moribund.
509
510 **ELISA**
511 MaxiSorp ELISA plates (ThermoScientific Nunc) were coated with 100 µl of 1µg/ml anti-mIL-2
512 (BD Pharmingen #554424) at 4ºC overnight. Coated plates were blocked with 200µl of blocking
513 solution (10%FBS in PBS) for 1hr at room temperature (RT) followed by incubation of culture
514 supernatant and mIL-2 at different concentrations as standard. After 1hr, plates were washed and
515 incubated with anti-mIL-2-biotin (BD Pharmingen #554426) at RT for 1hr. After 1hr, plates were
516 incubated with 100µl of horseradish peroxidase-labeled avidin (Vector Laboratory, #A-2004)
517 1µg/ml for 30min. After washing, samples were developed using the KPL TMB Peroxidase
518 substrate system (Seracare #5120-0047) and read at 405 or 450 nm after the addition of the stop
519 solution.
520
521 **Quantitative RT-PCR**
522 RNA was isolated using the RNeasy Micro Kit (Qiagen 70004) following the manufacturer's
523 instructions. RNA was converted to cDNA using the High-Capacity cDNA Reverse Transcription
524 Kit (ThermoFisher Scientific #4368814) according to the manufacturer's instructions. The primers
525 of murine genes were purchased from Integrated DNA Technology (IDT). qPCR was performed
526 using the PowerUp SYBR Green Master Mix (ThermoFisher Scientific #A25780) and the Applied
527 Biosystems StepOnePlus 96-well real-time PCR system. Gene expression levels were calculated
528 based on the Delta-Delta Ct relative quantification method. Primers used for Nrn1 PCR were as
529 follows: GCGGTGCAAATAGCTTACCTG (forward); CGGTCTTGATGTTCGTCTTGTC
530 (reverse).
531
532 **Ca^{++} flux and Membrane potential measurement**
533 To measure Ca^{++} flux, CD4 cells were loaded with Fluo4 dye at 2µM in the complete cell culture
534 medium at 37ºC for 30min. Cells were washed and resuspended in HBSS Ca^{++} free medium and
535 plated into 384 well glass bottom assay plate (minimum of 4 wells per sample). Ca^{++} flux was

536 measured using the FDSS6000 system (Hamamatsu Photonics). To measure store-operated
537 calcium entry (SOCE), after the recording of the baseline T cells Ca^{++} fluorescent for 1min,
538 thapsigargin (TG) was added to induce store Ca^{++} depletion, followed by the addition of Ca^{++} 2μM
539 in the extracellular medium to observe Ca^{++} cellular entry.
540 Membrane potential was measured using FLIPR Membrane Potential Assay kit (Molecular devices)
541 according to the manufacturer's instructions. Specifically, T cells were loaded with FLIPR dye by
542 adding an equal volume of FLIPR dye to the cells and incubated at 37°C for 30 minutes. Relative
543 membrane potential was measured by detecting FLIPR dye incorporation using flow cytometry.
544
545 **Extracellular flux analysis (Seahorse assays).**
546 Real-time measurements of extracellular acidification rate (ECAR) and oxygen consumption rate
547 (OCR) were performed using an XFe-96 Bioanalyser (Agilent). T cells (2×10^5 cells per well;
548 minimum of four wells per sample) were spun into previously poly-d-lysine-coated 96-well plates
549 (Seahorse) in complete RPMI-1640 medium. ECAR was measured in RPMI medium in basal
550 condition and in response to 25mM glucose, 1μM oligomycin, and 50mM of 2-DG (all from Sigma
551 Aldrich). OCR was measured in RPMI medium supplemented with 25mM glucose, 2mM L-
552 glutamine, and 1mM sodium pyruvate, under basal condition and in response to 1μM oligomycin,
553 1.5μM of carbonylcyanide-4-(trifluoromethoxy)-phenylhydrazone (FCCP) and 1μM of rotenone
554 and antimycin (all from Sigma Aldrich).
555
556 **RNAseq and data analysis**
557 RNASeq samples: 1. Anergic T cell analysis. Ctrl and $Nrn1^{-/-}$ OTII cells were sorted from the host
558 mice (n=3 per group). 2. iTreg cell analysis. In vitro differentiated $Nrn1^{-/-}$ and ctrl iTreg cells were
559 replated in resting condition (IL2 100u/ml) or stimulation condition (IL2 100u/ml and aCD3
560 5ug/ml). Cells were harvested 20 hr after replating for RNASeq analysis. 3. Effector T cells. $Nrn1^{-}$
561 $^{/-}$ and ctrl CD4 Tn cells were activated for 3 days (aCD3 5ug/ml, aCD28 2ug/ml), followed by
562 replating in IL2 medium (100u/ml). Te cells were harvested two days after replating and subjected
563 to RNASeq analysis.
564 RNA-sequencing analysis was performed by Admera Health (South Plainfield, NJ). Read quality
565 was assessed with FastQC and aligned to the Mus Musculus genome (Ensembl GRCm38) using
566 STAR aligner (version 2.6.0)(Dobin et al., 2013). Aligned reads were counted using HTSeq

567 (version 0.9.0)(Anders et al., 2015), and the counts were loaded into R (The R Foundation).
568 DESeq2 package (version 1.24.0)(Love et al., 2014) was used to normalize the raw counts. GSEA
569 was performed using public gene sets (HALLMARK, and GO)(Subramanian et al., 2005).
570 Cytoscape was used to display enriched gene sets cluster (Shannon et al., 2003).
571 Statistical analysis. All numerical data were processed using Graph Pad Prism 10. Data are
572 expressed as the mean +/- the SEM, or as stated. Statistical comparisons were made using an
573 unpaired student t-test or ANOVA with multiple comparison tests where 0.05 was considered
574 significant, and a normal distribution was assumed. The p values are represented as follows: *
575 $p<0.05$; ** $p<0.01$; *** $p<0.001$, **** $p<0.0001$.
576
577 **Acknowledgements:**
578 This research is supported by grants from the Bloomberg-Kimmel Institute of JHU, the Melanoma
579 Research Alliance, the National Institutes of Health (RO1AI099300 and RO1AI089830), and the
580 Department of Defense (PC130767). JB's research was supported by a Crohn's and Colitis
581 Foundation of America Research Fellowship, the Melanoma Research Foundation, and NCI grant
582 P30CA016056.
583 We thank Dennis Gong for data processing and critical reading of the manuscript. We thank Dr.
584 Elly Nedivi for providing polyclonal Nrn1 antibody and Dr. Fan Pan for reagent support. We thank
585 Drs. Franck Housseau, Chien-Fu Hung for the constructive discussion of the project and the
586 manuscript. We thank Drs. Hao Shi and Hongbo Chi for critical manuscript reading and helpful
587 suggestions. We thank Dr. Rachel Helm for manuscript editing. We thank Drs. Richard L. Huganir,
588 Bian Liu and Hana Goldschmidt for constructive discussion on Nrn1 and AMPAR connection.
589 **Author contributions:**
590 H. Y. was involved in all aspects of this study, including planning and performing experiments,
591 analyzing and interpreting data, and writing the manuscript. H. N. and J. B. were involved in
592 performing experiments and data interpretation. P. V., Y. Z, and A. L. analyzed Nrn1 expression
593 in Treg cells and carried out Treg suppression and functional assay. M. M. was involved in Nrn1
594 expression, Treg suppression assay, and manuscript writing. C. H. and C.D. conducted the anergy
595 and Te cell differential gene expression study; Y.Z., J. F., and K. C. conducted an autoimmune
596 inflammation study, and M. H. helped with mouse colony genotyping. X. Z. and Z. L. contributed
597 to bioinformatic analysis. D.M. P. oversaw the project and was involved in data interpretation and

manuscript preparation.

Competing interests:

C.D. is a co-inventor on patents licensed from JHU to BMS and Janssen and is currently an employee of Janssen Research. D.M.P. is a consultant for Compugen, Shattuck Labs, WindMIL, Tempest, Immunai, Bristol-Myers Squibb, Amgen, Janssen, Astellas, Rockspring Capital, Immunomic, and Dracen; owns founders' equity in ManaT Bio Inc., WindMIL, Trex, Jounce, Enara, Tizona, Tieza, and RAPT; and receives research funding from Compugen, Bristol-Myers Squibb, and Enara. All other authors do not have conflicting financial interests.

Data availability:

The raw RNA sequencing data has been deposited under the GEO accession no. GSE121908 and GSE224083.

629 **References:**

630 Abdul Kadir, L., M. Stacey, and R. Barrett-Jolley. 2018. Emerging Roles of the Membrane
631 Potential: Action Beyond the Action Potential. *Front Physiol* 9:1661.
632 Adler, A.J., D.W. Marsh, G.S. Yochum, J.L. Guzzo, A. Nigam, W.G. Nelson, and D.M. Pardoll.
633 1998. CD4+ T cell tolerance to parenchymal self-antigens requires presentation by bone
634 marrow-derived antigen-presenting cells. *The Journal of experimental medicine*
635 187:1555-1564.
636 Anders, S., P.T. Pyl, and W. Huber. 2015. HTSeq--a Python framework to work with high-
637 throughput sequencing data. *Bioinformatics* 31:166-169.
638 Babst, M. 2020. Regulation of nutrient transporters by metabolic and environmental stresses.
639 *Curr Opin Cell Biol* 65:35-41.
640 Blackiston, D.J., K.A. McLaughlin, and M. Levin. 2009. Bioelectric controls of cell proliferation:
641 ion channels, membrane voltage and the cell cycle. *Cell Cycle* 8:3527-3536.
642 Bohmwald, K., N.M.S. Gálvez, C.A. Andrade, V.P. Mora, J.T. Muñoz, P.A. González, C.A. Riedel,
643 and A.M. Kalergis. 2021. Modulation of Adaptive Immunity and Viral Infections by Ion
644 Channels. *Front Physiol* 12:736681.
645 Bonnet, C.S., S.J. Gilbert, E.J. Blain, A.S. Williams, and D.J. Mason. 2020. AMPA/kainate
646 glutamate receptor antagonists prevent posttraumatic osteoarthritis. *JCI insight* 5:
647 Bonnet, C.S., A.S. Williams, S.J. Gilbert, A.K. Harvey, B.A. Evans, and D.J. Mason. 2015.
648 AMPA/kainate glutamate receptors contribute to inflammation, degeneration and pain
649 related behaviour in inflammatory stages of arthritis. *Annals of the rheumatic diseases*
650 74:242-251.
651 Buck, M.D., R.T. Sowell, S.M. Kaech, and E.L. Pearce. 2017. Metabolic Instruction of Immunity.
652 *Cell* 169:570-586.
653 Cantallops, I., K. Haas, and H.T. Cline. 2000. Postsynaptic CPG15 promotes synaptic maturation
654 and presynaptic axon arbor elaboration in vivo. *Nature neuroscience* 3:1004-1011.
655 Chapman, N.M., and H. Chi. 2022. Metabolic adaptation of lymphocytes in immunity and
656 disease. *Immunity* 55:14-30.
657 Chappert, P., and R.H. Schwartz. 2010. Induction of T cell anergy: integration of environmental
658 cues and infectious tolerance. *Current opinion in immunology* 22:552-559.
659 Chen, T.C., S.P. Cobbold, P.J. Fairchild, and H. Waldmann. 2004. Generation of anergic and
660 regulatory T cells following prolonged exposure to a harmless antigen. *Journal of*
661 *immunology (Baltimore, Md. : 1950)* 172:5900-5907.
662 Choi, S., and R.H. Schwartz. 2007. Molecular mechanisms for adaptive tolerance and other T cell
663 anergy models. *Seminars in immunology* 19:140-152.
664 Cuenca, A., F. Cheng, H. Wang, J. Brayer, P. Horna, L. Gu, H. Bien, I.M. Borrello, H.I. Levitsky, and
665 E.M. Sotomayor. 2003. Extra-lymphatic solid tumor growth is not immunologically
666 ignored and results in early induction of antigen-specific T-cell anergy: dominant role of
667 cross-tolerance to tumor antigens. *Cancer research* 63:9007-9015.
668 DL, K.L.a.M. 2017. Relationship between CD4 Regulatory T Cells and Anergy In Vivo. *Journal of*
669 *immunology (Baltimore, Md. : 1950)* 198:2527.
670 Dobin, A., C.A. Davis, F. Schlesinger, J. Drenkow, C. Zaleski, S. Jha, P. Batut, M. Chaisson, and
671 T.R. Gingeras. 2013. STAR: ultrafast universal RNA-seq aligner. *Bioinformatics* 29:15-21.

672 Dvorak, V., T. Wiedmer, A. Ingles-Prieto, P. Altermatt, H. Batoulis, F. Bärenz, E. Bender, D.
673 Digles, F. Dürrenberger, L.H. Heitman, I.J. AP, D.B. Kell, S. Kickinger, D. Körzö, P. Leippe,
674 T. Licher, V. Manolova, R. Rizzetto, F. Sassone, L. Scarabottolo, A. Schlessinger, V.
675 Schneider, H.J. Sijben, A.L. Steck, H. Sundström, S. Tremolada, M. Wilhelm, M. Wright
676 Muelas, D. Zindel, C.M. Steppan, and G. Superti-Furga. 2021. An Overview of Cell-Based
677 Assay Platforms for the Solute Carrier Family of Transporters. *Frontiers in pharmacology*
678 12:722889.
679 ElTanbouly, M.A., and R.J. Noelle. 2021. Rethinking peripheral T cell tolerance: checkpoints
680 across a T cell's journey. *Nat Rev Immunol* 21:257-267.
681 Emmons-Bell, M., and I.K. Hariharan. 2021. Membrane potential regulates Hedgehog signalling
682 in the Drosophila wing imaginal disc. *EMBO reports* 22:e51861.
683 Feng, Y., A. Arvey, T. Chinen, J. van der Veeken, G. Gasteiger, and A.Y. Rudensky. 2014. Control
684 of the inheritance of regulatory T cell identity by a cis element in the Foxp3 locus. *Cell*
685 158:749-763.
686 Floess, S., J. Freyer, C. Siewert, U. Baron, S. Olek, J. Polansky, K. Schlawe, H.D. Chang, T. Bopp, E.
687 Schmitt, S. Klein-Hessling, E. Serfling, A. Hamann, and J. Huehn. 2007. Epigenetic control
688 of the foxp3 locus in regulatory T cells. *PLoS biology* 5:e38.
689 Fujino, T., J.H. Leslie, R. Eavri, J.L. Chen, W.C. Lin, G.H. Flanders, E. Borok, T.L. Horvath, and E.
690 Nedivi. 2011. CPG15 regulates synapse stability in the developing and adult brain. *Genes*
691 *& development* 25:2674-2685.
692 Geltink, R.I.K., R.L. Kyle, and E.L. Pearce. 2018. Unraveling the Complex Interplay Between T Cell
693 Metabolism and Function. *Annual review of immunology* 36:461-488.
694 Gonzalez-Figueroa, P., J.A. Roco, I. Papa, L. Núñez Villacís, M. Stanley, M.A. Linterman, A. Dent,
695 P.F. Canete, and C.G. Vinuesa. 2021. Follicular regulatory T cells produce neuritin to
696 regulate B cells. *Cell*
697 Hamill, M.J., R. Afeyan, M.V. Chakravarthy, and T. Tramontin. 2020. Endogenous Metabolic
698 Modulators: Emerging Therapeutic Potential of Amino Acids. *iScience* 23:101628.
699 Huang, C.T., D.L. Huso, Z. Lu, T. Wang, G. Zhou, E.P. Kennedy, C.G. Drake, D.J. Morgan, L.A.
700 Sherman, A.D. Higgins, D.M. Pardoll, and A.J. Adler. 2003. CD4+ T cells pass through an
701 effector phase during the process of in vivo tolerance induction. *Journal of immunology*
702 *(Baltimore, Md. : 1950)* 170:3945-3953.
703 Huang, C.T., C.J. Workman, D. Flies, X. Pan, A.L. Marson, G. Zhou, E.L. Hipkiss, S. Ravi, J.
704 Kowalski, H.I. Levitsky, J.D. Powell, D.M. Pardoll, C.G. Drake, and D.A. Vignali. 2004. Role
705 of LAG-3 in regulatory T cells. *Immunity* 21:503-513.
706 Javaherian, A., and H.T. Cline. 2005. Coordinated motor neuron axon growth and
707 neuromuscular synaptogenesis are promoted by CPG15 in vivo. *Neuron* 45:505-512.
708 Joesch, C., E. Guevarra, S.P. Parel, A. Bergner, P. Zbinden, D. Konrad, and H. Albrecht. 2008. Use
709 of FLIPR membrane potential dyes for validation of high-throughput screening with the
710 FLIPR and microARCS technologies: identification of ion channel modulators acting on
711 the GABA(A) receptor. *J Biomol Screen* 13:218-228.
712 Kalekar, L.A., S.E. Schmiel, S.L. Nandiwada, W.Y. Lam, L.O. Barsness, N. Zhang, G.L. Stritesky, D.
713 Malhotra, K.E. Pauken, J.L. Linehan, M.G. O'Sullivan, B.T. Fife, K.A. Hogquist, M.K.
714 Jenkins, and D.L. Mueller. 2016. CD4(+) T cell anergy prevents autoimmunity and
715 generates regulatory T cell precursors. *Nature immunology* 17:304-314.

716 Kiefer, H., A.J. Blume, and H.R. Kaback. 1980. Membrane potential changes during mitogenic
717 stimulation of mouse spleen lymphocytes. *Proceedings of the National Academy of*
718 *Sciences of the United States of America* 77:2200-2204.
719 Kim, J.M., J.P. Rasmussen, and A.Y. Rudensky. 2007. Regulatory T cells prevent catastrophic
720 autoimmunity throughout the lifespan of mice. *Nature immunology* 8:191-197.
721 Kuczma, M.P., E.A. Szurek, A. Cebula, V.L. Ngo, M. Pietrzak, P. Kraj, T.L. Denning, and L.
722 Ignatowicz. 2021. Self and microbiota-derived epitopes induce CD4(+) T cell anergy and
723 conversion into CD4(+)Foxp3(+) regulatory cells. *Mucosal Immunol* 14:443-454.
724 Levin, M. 2021. Bioelectric signaling: Reprogrammable circuits underlying embryogenesis,
725 regeneration, and cancer. *Cell* 184:1971-1989.
726 Li, X., Y. Liang, M. LeBlanc, C. Benner, and Y. Zheng. 2014. Function of a Foxp3 cis-element in
727 protecting regulatory T cell identity. *Cell* 158:734-748.
728 Lim, D.G., Y.H. Park, S.E. Kim, S.H. Jeong, and S.C. Kim. 2013. Diagnostic value of tolerance-
729 related gene expression measured in the recipient alloantigen-reactive T cell fraction.
730 *Clinical immunology (Orlando, Fla.)* 148:219-226.
731 Liu, G.Y., and D.M. Sabatini. 2020. mTOR at the nexus of nutrition, growth, ageing and disease.
732 *Nat Rev Mol Cell Biol* 21:183-203.
733 Long, L., J. Wei, S.A. Lim, J.L. Raynor, H. Shi, J.P. Connelly, H. Wang, C. Guy, B. Xie, N.M.
734 Chapman, G. Fu, Y. Wang, H. Huang, W. Su, J. Saravia, I. Risch, Y.D. Wang, Y. Li, M. Niu, Y.
735 Dhungana, A. Kc, P. Zhou, P. Vogel, J. Yu, S.M. Pruett-Miller, J. Peng, and H. Chi. 2021.
736 CRISPR screens unveil signal hubs for nutrient licensing of T cell immunity. *Nature*
737 600:308-313.
738 Love, M.I., W. Huber, and S. Anders. 2014. Moderated estimation of fold change and dispersion
739 for RNA-seq data with DESeq2. *Genome biology* 15:550.
740 Ma, Y., K. Poole, J. Goyette, and K. Gaus. 2017. Introducing Membrane Charge and Membrane
741 Potential to T Cell Signaling. *Frontiers in immunology* 8:1513.
742 Martinez, R.J., N. Zhang, S.R. Thomas, S.L. Nandiwada, M.K. Jenkins, B.A. Binstadt, and D.L.
743 Mueller. 2012. Arthritogenic self-reactive CD4+ T cells acquire an FR4hiCD73hi anergic
744 state in the presence of Foxp3+ regulatory T cells. *Journal of immunology (Baltimore,*
745 *Md. : 1950)* 188:170-181.
746 McNearney, T., B.A. Baethge, S. Cao, R. Alam, J.R. Lisse, and K.N. Westlund. 2004. Excitatory
747 amino acids, TNF-alpha, and chemokine levels in synovial fluids of patients with active
748 arthropathies. *Clinical and experimental immunology* 137:621-627.
749 Mercadante, E.R., and U.M. Lorenz. 2016. Breaking Free of Control: How Conventional T Cells
750 Overcome Regulatory T Cell Suppression. *Frontiers in immunology* 7:193.
751 Miller, S.D., W.J. Karpus, and T.S. Davidson. 2007. Experimental Autoimmune Encephalomyelitis
752 in the Mouse. *Current protocols in immunology* CHAPTER:Unit-15 11.
753 Monroe, J.G., and J.C. Cambier. 1983. B cell activation. I. Anti-immunoglobulin-induced receptor
754 cross-linking results in a decrease in the plasma membrane potential of murine B
755 lymphocytes. *The Journal of experimental medicine* 157:2073-2086.
756 Nedivi, E., G.Y. Wu, and H.T. Cline. 1998. Promotion of dendritic growth by CPG15, an activity-
757 induced signaling molecule. *Science (New York, N.Y.)* 281:1863-1866.

758 Nik, A.M., B. Pressly, V. Singh, S. Antrobus, S. Hulsizer, M.A. Rogawski, H. Wulff, and I.N. Pessah.
759 2017. Rapid Throughput Analysis of GABA(A) Receptor Subtype Modulators and Blockers
760 Using DiSBAC(1)(3) Membrane Potential Red Dye. *Mol Pharmacol* 92:88-99.
761 Nystrom, S.N., D. Bourges, S. Garry, E.M. Ross, I.R. van Driel, and P.A. Gleeson. 2014. Transient
762 Treg-cell depletion in adult mice results in persistent self-reactive CD4(+) T-cell
763 responses. *European journal of immunology* 44:3621-3631.
764 Olenchock, B.A., J.C. Rathmell, and M.G. Vander Heiden. 2017. Biochemical Underpinnings of
765 Immune Cell Metabolic Phenotypes. *Immunity* 46:703-713.
766 Opejin, A., A. Surnov, Z. Misulovin, M. Pherson, C. Gross, C.A. Iberg, I. Fallahee, J. Bourque, D.
767 Dorsett, and D. Hawiger. 2020. A Two-Step Process of Effector Programming Governs
768 CD4(+) T Cell Fate Determination Induced by Antigenic Activation in the Steady State.
769 *Cell reports* 33:108424.
770 Pandya, N.J., C. Seeger, N. Babai, M.A. Gonzalez-Lozano, V. Mack, J.C. Lodder, Y. Gouwenberg,
771 H.D. Mansvelder, U.H. Danielson, K.W. Li, M. Heine, S. Spijker, R. Frischknecht, and A.B.
772 Smit. 2018. Noelin1 Affects Lateral Mobility of Synaptic AMPA Receptors. *Cell reports*
773 24:1218-1230.
774 Peng, M., and M.O. Li. 2023. Metabolism along the life journey of T cells. *Life Metab* 2:
775 Plitas, G., C. Konopacki, K. Wu, P.D. Bos, M. Morrow, E.V. Putintseva, D.M. Chudakov, and A.Y.
776 Rudensky. 2016. Regulatory T Cells Exhibit Distinct Features in Human Breast Cancer.
777 *Immunity* 45:1122-1134.
778 Putz, U., C. Harwell, and E. Nedivi. 2005. Soluble CPG15 expressed during early development
779 rescues cortical progenitors from apoptosis. *Nature neuroscience* 8:322-331.
780 Ramirez, G.A., L.A. Coletto, C. Sciorati, E.P. Bozzolo, P. Manunta, P. Rovere-Querini, and A.A.
781 Manfredi. 2018. Ion Channels and Transporters in Inflammation: Special Focus on TRP
782 Channels and TRPC6. *Cells* 7:
783 Safford, M., S. Collins, M.A. Lutz, A. Allen, C.T. Huang, J. Kowalski, A. Blackford, M.R. Horton, C.
784 Drake, R.H. Schwartz, and J.D. Powell. 2005. Egr-2 and Egr-3 are negative regulators of T
785 cell activation. *Nature immunology* 6:472-480.
786 Salmond, R.J. 2018. mTOR Regulation of Glycolytic Metabolism in T Cells. *Frontiers in cell and*
787 *developmental biology* 6:122.
788 Saravia, J., J.L. Raynor, N.M. Chapman, S.A. Lim, and H. Chi. 2020. Signaling networks in
789 immunometabolism. *Cell research* 30:328-342.
790 Sarchielli, P., M. Di Filippo, A. Candeliere, D. Chiasserini, A. Mattioni, S. Tenaglia, M. Bonucci,
791 and P. Calabresi. 2007. Expression of ionotropic glutamate receptor GLUR3 and effects
792 of glutamate on MBP- and MOG-specific lymphocyte activation and chemotactic
793 migration in multiple sclerosis patients. *Journal of neuroimmunology* 188:146-158.
794 Schietinger, A., J.J. Delrow, R.S. Basom, J.N. Blattman, and P.D. Greenberg. 2012. Rescued
795 tolerant CD8 T cells are preprogrammed to reestablish the tolerant state. *Science (New*
796 *York, N.Y.)* 335:723-727.
797 Schietinger, A., M. Philip, V.E. Krisnawan, E.Y. Chiu, J.J. Delrow, R.S. Basom, P. Lauer, D.G.
798 Brockstedt, S.E. Knoblaugh, G.J. Hammerling, T.D. Schell, N. Garbi, and P.D. Greenberg.
799 2016. Tumor-Specific T Cell Dysfunction Is a Dynamic Antigen-Driven Differentiation
800 Program Initiated Early during Tumorigenesis. *Immunity* 45:389-401.

801 Schwenk, J., N. Harmel, A. Brechet, G. Zolles, H. Berkefeld, C.S. Muller, W. Bildl, D. Baehrens, B.
802 Huber, A. Kulik, N. Klocker, U. Schulte, and B. Fakler. 2012. High-resolution proteomics
803 unravel architecture and molecular diversity of native AMPA receptor complexes.
804 *Neuron* 74:621-633.
805 Shannon, P., A. Markiel, O. Ozier, N.S. Baliga, J.T. Wang, D. Ramage, N. Amin, B. Schwikowski,
806 and T. Ideker. 2003. Cytoscape: a software environment for integrated models of
807 biomolecular interaction networks. *Genome Res* 13:2498-2504.
808 Shimada, T., T. Yoshida, and K. Yamagata. 2016. Neuritin Mediates Activity-Dependent Axonal
809 Branch Formation in Part via FGF Signaling. *The Journal of neuroscience : the official*
810 *journal of the Society for Neuroscience* 36:4534-4548.
811 Shin, D.S., A. Jordan, S. Basu, R.M. Thomas, S. Bandyopadhyay, E.F. de Zoeten, A.D. Wells, and F.
812 Macian. 2014. Regulatory T cells suppress CD4+ T cells through NFAT-dependent
813 transcriptional mechanisms. *EMBO reports* 15:991-999.
814 Silva Morales, M., and D. Mueller. 2018. Anergy into T regulatory cells: an integration of
815 metabolic cues and epigenetic changes at the Foxp3 conserved non-coding sequence 2.
816 *F1000Research* 7:
817 Sinclair, L.V., J. Rolf, E. Emslie, Y.B. Shi, P.M. Taylor, and D.A. Cantrell. 2013. Control of amino-
818 acid transport by antigen receptors coordinates the metabolic reprogramming essential
819 for T cell differentiation. *Nature immunology* 14:500-508.
820 Singer, M., C. Wang, L. Cong, N.D. Marjanovic, M.S. Kowalczyk, H. Zhang, J. Nyman, K. Sakuishi,
821 S. Kurtulus, D. Gennert, J. Xia, J.Y. Kwon, J. Nevin, R.H. Herbst, I. Yanai, O. Rozenblatt-
822 Rosen, V.K. Kuchroo, A. Regev, and A.C. Anderson. 2016. A Distinct Gene Module for
823 Dysfunction Uncoupled from Activation in Tumor-Infiltrating T Cells. *Cell* 166:1500-
824 1511.e1509.
825 Subramanian, A., P. Tamayo, V.K. Mootha, S. Mukherjee, B.L. Ebert, M.A. Gillette, A. Paulovich,
826 S.L. Pomeroy, T.R. Golub, E.S. Lander, and J.P. Mesirov. 2005. Gene set enrichment
827 analysis: a knowledge-based approach for interpreting genome-wide expression
828 profiles. *Proceedings of the National Academy of Sciences of the United States of*
829 *America* 102:15545-15550.
830 Subramanian, J., K. Michel, M. Benoit, and E. Nedivi. 2019. CPG15/Neuritin Mimics Experience
831 in Selecting Excitatory Synapses for Stabilization by Facilitating PSD95 Recruitment. *Cell*
832 *reports* 28:1584-1595.e1585.
833 Sullivan, M.R., L.V. Danai, C.A. Lewis, S.H. Chan, D.Y. Gui, T. Kunchok, E.A. Dennstedt, M.G.
834 Vander Heiden, and A. Muir. 2019. Quantification of microenvironmental metabolites in
835 murine cancers reveals determinants of tumor nutrient availability. *eLife* 8:
836 Sundelacruz, S., M. Levin, and D.L. Kaplan. 2009. Role of membrane potential in the regulation
837 of cell proliferation and differentiation. *Stem Cell Rev Rep* 5:231-246.
838 Vahl, J.C., C. Drees, K. Heger, S. Heink, J.C. Fischer, J. Nedjic, N. Ohkura, H. Morikawa, H. Poeck,
839 S. Schallenberg, D. Riess, M.Y. Hein, T. Buch, B. Polic, A. Schonle, R. Zeiser, A. Schmitt-
840 Graff, K. Kretschmer, L. Klein, T. Korn, S. Sakaguchi, and M. Schmidt-Supprian. 2014.
841 Continuous T cell receptor signals maintain a functional regulatory T cell pool. *Immunity*
842 41:722-736.

843 Vanasek, T.L., S.L. Nandiwada, M.K. Jenkins, and D.L. Mueller. 2006. CD25+Foxp3+ regulatory T
844 cells facilitate CD4+ T cell clonal anergy induction during the recovery from
845 lymphopenia. *Journal of immunology (Baltimore, Md. : 1950)* 176:5880-5889.
846 Wang, Y., A. Tao, M. Vaeth, and S. Feske. 2020. Calcium regulation of T cell metabolism. *Current*
847 *opinion in physiology* 17:207-223.
848 Whiteaker, K.L., S.M. Gopalakrishnan, D. Groebe, C.C. Shieh, U. Warrior, D.J. Burns, M.J.
849 Coghlan, V.E. Scott, and M. Gopalakrishnan. 2001. Validation of FLIPR membrane
850 potential dye for high throughput screening of potassium channel modulators. *J Biomol*
851 *Screen* 6:305-312.
852 Workman, C.J., L.W. Collison, M. Bettini, M.R. Pillai, J.E. Rehg, and D.A. Vignali. 2011. In vivo
853 Treg suppression assays. *Methods in molecular biology (Clifton, N.J.)* 707:119-156.
854 Yao, J.J., X.F. Gao, C.W. Chow, X.Q. Zhan, C.L. Hu, and Y.A. Mei. 2012. Neuritin activates insulin
855 receptor pathway to up-regulate Kv4.2-mediated transient outward K+ current in rat
856 cerebellar granule neurons. *The Journal of biological chemistry* 287:41534-41545.
857 Yu, W., Z. Wang, X. Yu, Y. Zhao, Z. Xie, K. Zhang, Z. Chi, S. Chen, T. Xu, D. Jiang, X. Guo, M. Li, J.
858 Zhang, H. Fang, D. Yang, Y. Guo, X. Yang, X. Zhang, Y. Wu, W. Yang, and D. Wang. 2022.
859 Kir2.1-mediated membrane potential promotes nutrient acquisition and inflammation
860 through regulation of nutrient transporters. *Nature communications* 13:3544.
861 Zha, Y., R. Marks, A.W. Ho, A.C. Peterson, S. Janardhan, I. Brown, K. Praveen, S. Stang, J.C.
862 Stone, and T.F. Gajewski. 2006. T cell anergy is reversed by active Ras and is regulated
863 by diacylglycerol kinase-alpha. *Nature immunology* 7:1166-1173.
864 Zheng, Y., G.M. Delgoffe, C.F. Meyer, W. Chan, and J.D. Powell. 2009. Anergic T cells are
865 metabolically anergic. *Journal of immunology (Baltimore, Md. : 1950)* 183:6095-6101.
866 Zheng, Y., S. Josefowicz, A. Chaudhry, X.P. Peng, K. Forbush, and A.Y. Rudensky. 2010. Role of
867 conserved non-coding DNA elements in the Foxp3 gene in regulatory T-cell fate. *Nature*
868 463:808-812.
869 Zhou, S., and J. Zhou. 2014. Neuritin, a neurotrophic factor in nervous system physiology.
870 *Current medicinal chemistry* 21:1212-1219.
871 Zhou, Y., C.O. Wong, K.J. Cho, D. van der Hoeven, H. Liang, D.P. Thakur, J. Luo, M. Babic, K.E.
872 Zinsmaier, M.X. Zhu, H. Hu, K. Venkatachalam, and J.F. Hancock. 2015. SIGNAL
873 TRANSDUCTION. Membrane potential modulates plasma membrane phospholipid
874 dynamics and K-Ras signaling. *Science (New York, N.Y.)* 349:873-876.
875 Zito, A., D. Cartelli, G. Cappelletti, A. Cariboni, W. Andrews, J. Parnavelas, A. Poletti, and M.
876 Galbiati. 2014. Neuritin 1 promotes neuronal migration. *Brain Structure and Function*
877 219:105-118.
878
879
880
881
882
883

Main Figures

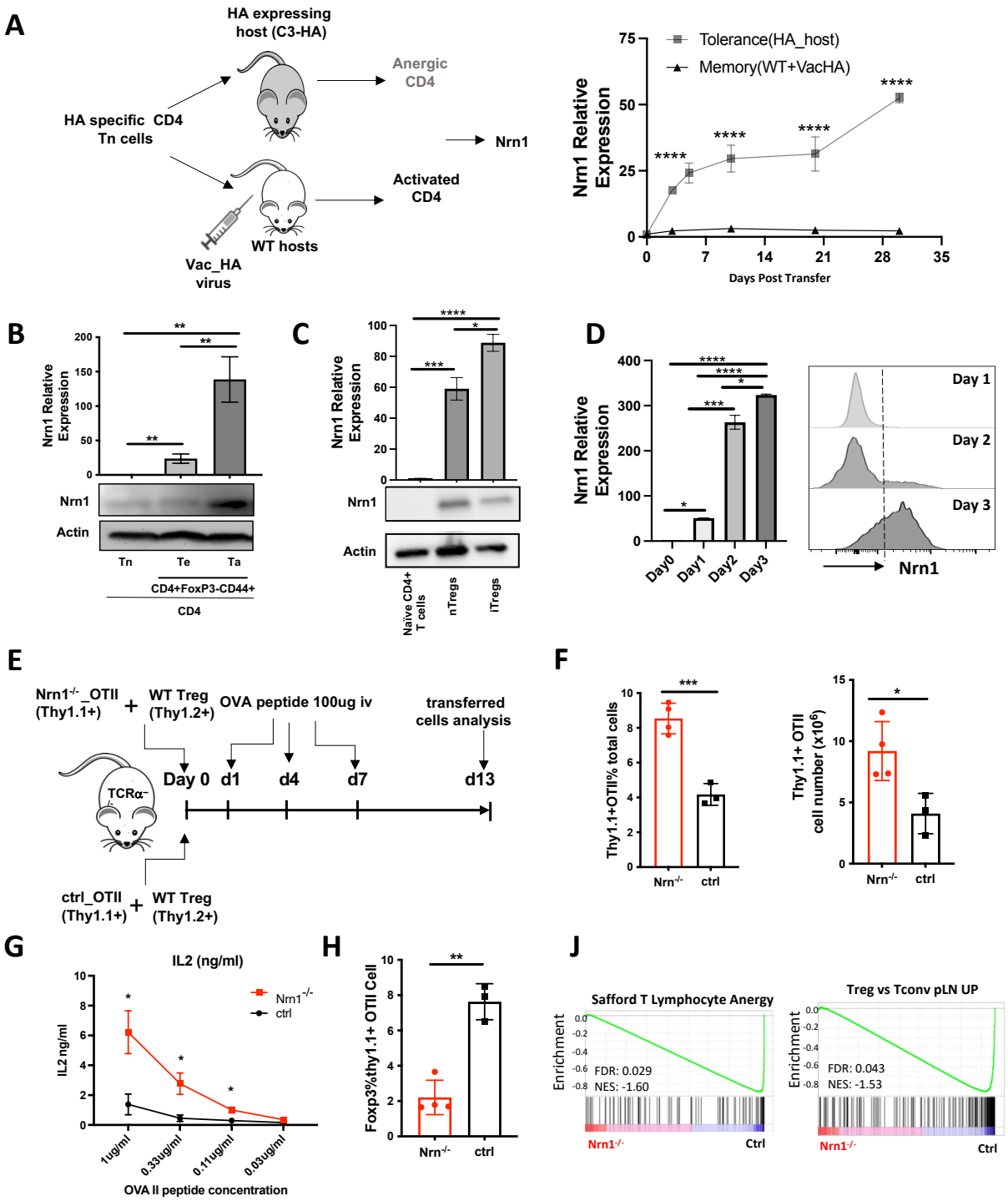

Figure 1. Nrn1 expression and function in anergic T cells.

(**A**) Experimental scheme identifying Nrn1 in anergic T cells and qRT-PCR confirmation of Nrn1 expression in HA-specific CD4 cells recovered from HA-expressing host vs WT host activated with Vac_HA virus. (**B**) qRT-PCR and western blot detecting Nrn1 expression in naïve

890 $CD4^+CD62L^{hi}CD44^{lo}$ Tn cell, $CD4^+Foxp3^-CD44^{hi}CD73^-FR^-$ Te cells and $CD4^+Foxp3^-$
891 $CD44^{hi}CD73^+FR^+$ Ta cells. (**C**) Nrn1 expression was measured by qRT-PCR and western blot
892 among naïve $CD4^+$ T cells, $CD4^+Foxp3^+$ nTreg, and *in vitro* generated iTregs. (**D**) Nrn1 expression
893 was detected by qRT-PCR and flow cytometry among naïve $CD4^+$ cells and activated $CD4^+$ cells
894 on days 1, 2, and 3 after activation. qPCR Data are presented as average $\pm$ SEM. *p<0.05,
895 **p<0.01, ***p<0.001, ****p<0.0001. Triplicates were used. Ordinary one-way ANOVA was
896 performed for multi-comparison.
897 (**E-J**). Anergy induction *in vivo*. (**E**) Experimental outline evaluating anergy development *in vivo*:
898 $2x10^6$ $Thy1.1^+$ $Nrn1^{-/-}$ or ctrl CD4 OTII T cells were co-transferred with $5x10^5$ $Thy1.2^+Thy1.1^-$
899 WT Treg cells into $TCR\alpha^{-/-}$mice. Cells were recovered on day 13 post-transfer. (**F**) Proportions
900 and numbers of OTII cells recovered from recipient spleen; (**G**) IL2 secretion from OTII cells
901 upon *ex vivo* stimulation with OVA peptide. (**H**) $Foxp3^+$ cell proportion among $Thy1.1^+$ $Nrn1^{-/-}$ or
902 ctrl CD4 cells. (**I & J**) $Nrn1^{-/-}$ vs ctrl OTII cells recovered from the peptide-induced anergy model
903 were subjected to bulk RNASeq analysis. GSEA comparing the expression of signature genes for
904 anergy (**I**) and Treg (**J**) among ctrl and $Nrn1^{-/-}$ OTII cells.
905 Data are presented as mean $\pm$SEM and representative of 3 independent experiments ($N \geq 4$ mice
906 per group). *p<0.05, **p<0.01, ***p<0.001. Unpaired Student's t-tests were performed.
907

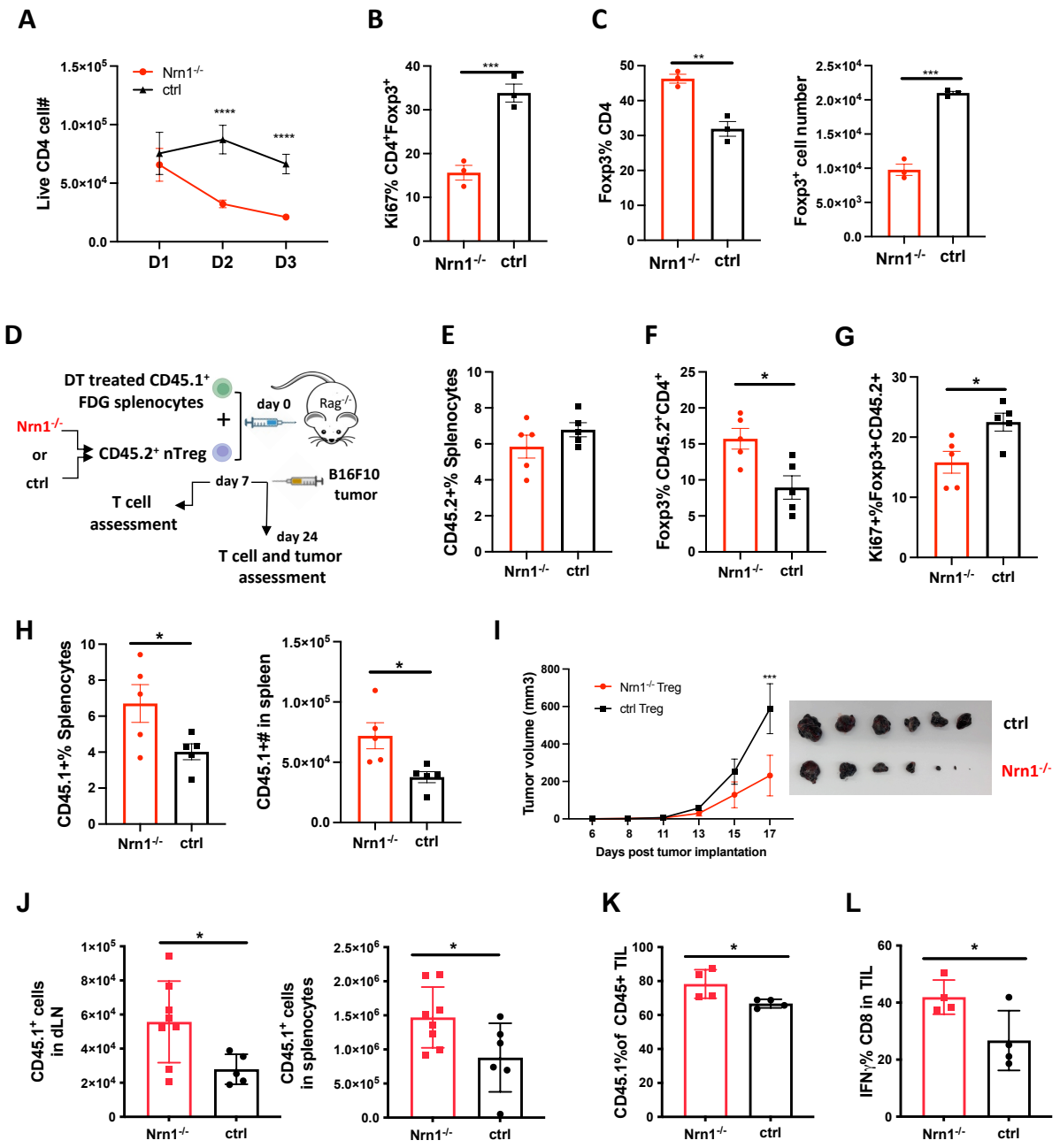

Figure 2. Reduced proliferation and suppression function in Nrn1$^{-/-}$ Treg cells.

(**A-C**) iTreg cell expansion after restimulation. (**A**) The number of live cells from day 1 to day 3 after iTreg cell restimulation with anti-CD3. (**B**) Ki67 expression among CD4^{+}Foxp3^{+} cells day 3 after restimulation. (**C**) Foxp3^{+} cell proportion and number among live CD4^{+} cells day 3 after restimulation. Triplicates in each experiment, data represent one of four independent experiments. (**D-L**). Nrn1$^{-/-}$ or ctrl nTreg cells expansion and suppression *in vivo*. (**D**) The experimental scheme. CD45.2^{+} nTreg T cells from Nrn1$^{-/-}$ or ctrl were transferred with CD45.1^{+} FDG splenocytes devoid

916 of Tregs into Rag2$^{-/-}$ host. Treg cell expansion and suppression toward FDG CD45.1^{+} responder
917 cells were evaluated on day 7 post cell transfer. Alternatively, B16F10 tumor cells were inoculated
918 on day 7 after cell transfer and monitored for tumor growth. (**E-H**) CD45.2^{+} cell proportion (**E**),
919 Foxp3 retention (**F**), and Ki67 expression among Foxp3^{+} cells (**G**) at day 7 post cell transfer. (**H**)
920 CD45.1^{+} cell proportion and number in the spleen of Nrn1$^{-/-}$ or ctrl Treg hosts day 7 post cell
921 transfer. (**I-L**)**.** Treg cell suppression toward anti-tumor response. (**I**) Tumor growth curve and
922 tumor size at harvest from Nrn1$^{-/-}$ or ctrl nTreg hosts. (**J**) CD45.1^{+} cell count in tumor draining
923 lymph node (LN) and spleen. (**K**) the proportion of CD45.1^{+} cells among CD45^{+} tumor
924 lymphocyte infiltrates (TILs). (**L**) IFNγ% among CD8^{+} T cells in TILs. n$\geq$5 mice per group. (**E-**
925 **H**) represents three independent experiments, **(I-L**) represents two independent experiments. Data
926 are presented as mean $\pm$SEM *p<0.05, **p<0.01, ***p<0.001, ****p<0.0001. Unpaired Student's
927 t-tests were performed.
928
929

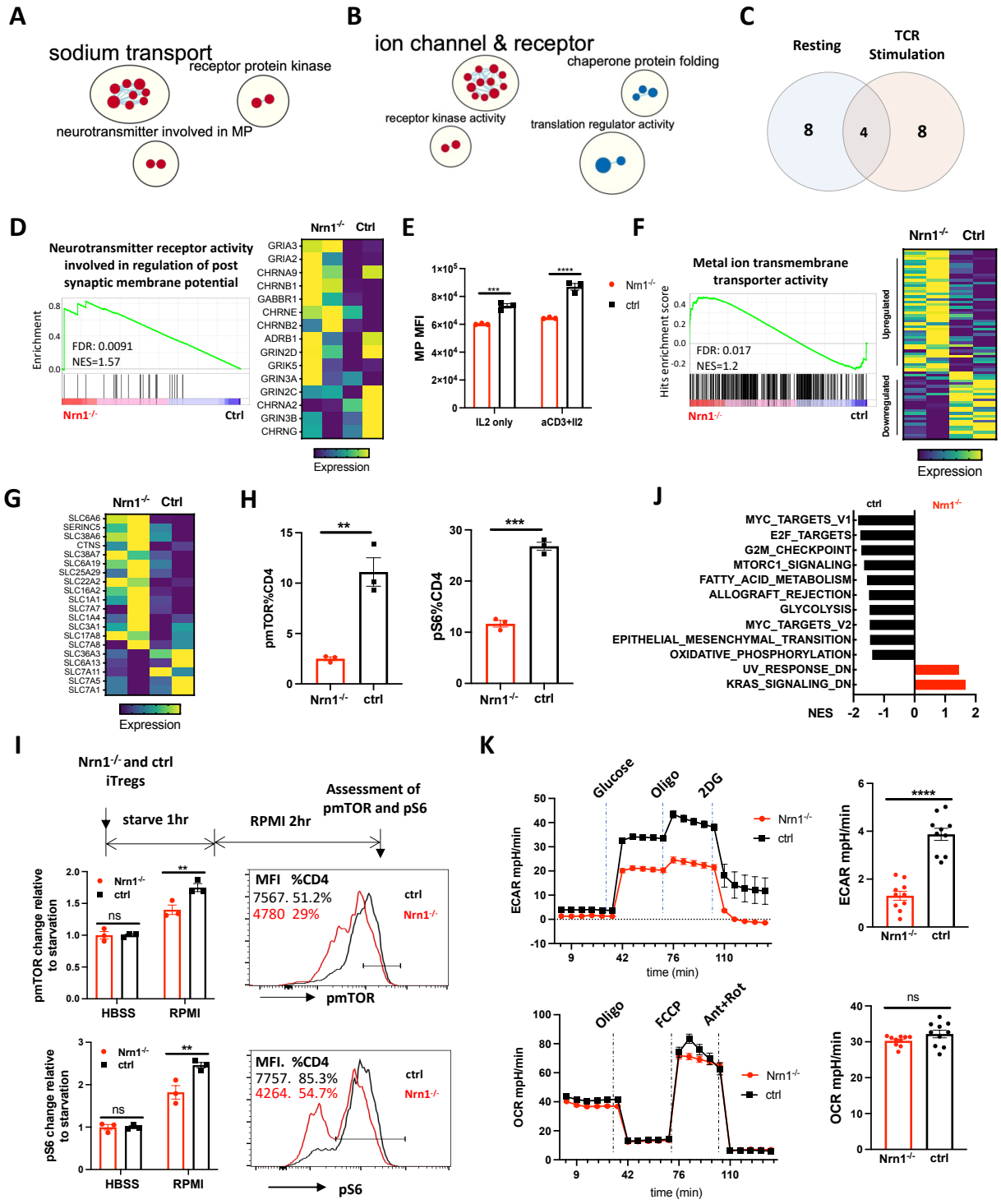

Figure.3. Nrn1 expression impacts Treg cell electrical and metabolic state.

(**A-C**). Gene sets clusters enriched in Nrn1$^{-/-}$ and ctrl iTreg cells. Gene sets cluster analysis via Cytoscape was performed on Gene ontology Molecular Function (GO_MF) gene sets. The results cutoff: p-value ≤0.05 and FDR q-value ≤0.1. (**A**) Gene sets cluster in Nrn1$^{-/-}$ iTreg cells cultured

935 under resting condition (IL2 only) (Figure 3-figure supplement Table 1). (**B**) Gene sets clusters in
936 Nrn1$^{-/-}$ and ctrl iTreg cells reactivated with anti-CD3 (Figure 3-figure supplement Table 2). (**C**)
937 Comparison of enriched gene sets in Nrn1$^{-/-}$ under resting vs. activating condition (Figure 3-figure
938 supplement Table 3). (**D-F)** Changes relating to cell electric state. (**D**) Enrichment of
939 "GOMF_Neurotransmitter receptor activity involved in the regulation of postsynaptic membrane
940 potential" gene set and enriched gene expression heatmap. (**E**) Membrane potential was measured
941 in Nrn1$^{-/-}$ and ctrl iTreg cells cultured in IL2 or activated with anti-CD3 in the presence of IL2.
942 Data represent three independent experiments. (**F**) Enrichment of "GOMF_Metal ion
943 transmembrane transporter activity" gene set and enriched gene expression heatmap (Figure 3-
944 figure supplement 1A). (**G-K**). Metabolic changes associated with Nrn1$^{-/-}$ iTreg. (**G**) Heatmap of
945 differentially expressed amino acid (AA) transport-related genes (from "MF_Amino acid
946 transmembrane transporter activity" gene list) in Nrn1$^{-/-}$ and ctrl iTreg cells. (**H**) pmTOR and pS6
947 levels in TCR activated iTreg cells measured by flow cytometry. n=3 replicates per group. Data
948 represent three independent experiments. (**I**) Measurement of pmTOR and pS6 in iTreg cells that
949 were deprived of nutrients for 1h and refed with RPMI for two hours. (**J**) Hallmark gene sets
950 significantly enriched in Nrn1$^{-/-}$ and ctrl iTreg. NOM p-val<0.05, FDR q-val<0.25. (**K**) Seahorse
951 analysis of extracellular acidification rate (ECAR) and oxygen consumption rate (OCR) in Nrn1$^{-/-}$
952 and ctrl iTreg cells. n=6~10 technical replicates per group. Data represent three independent
953 experiments. **p<0.01, ***p<0.001, ****p<0.0001. Unpaired student t-test for two-group
954 comparison. Unpaired t-test (H, K), two-way ANOVA (E, I). ns, not significant.
955

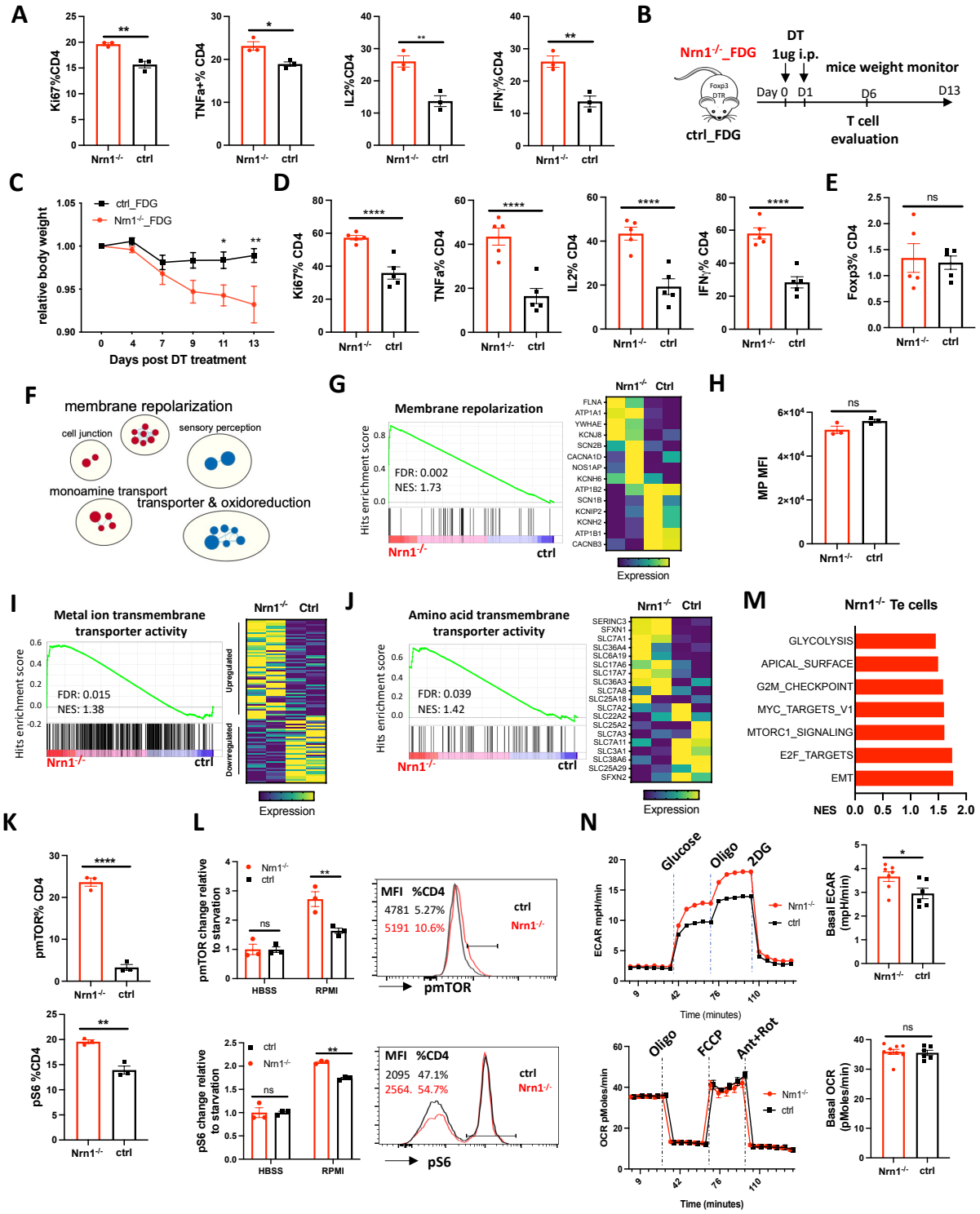

Figure 4. Nrn1 deficiency affects Te cell response.

(**A**) Comparison of cell proliferation and cytokine expression in Nrn1$^{-/-}$ and ctrl Te cells. Data represent one of three independent experiments. (**B-E**) An enhanced autoimmune response in Nrn1$^{-/-}$ mice *in vivo*. (**B**) Experimental scheme. Nrn1$^{-/-}$ mice were crossed with FDG mice and

961 Nrn1-/-_FDG or ctrl_FDG mice were obtained. The autoimmune response was induced by
962 injecting DT i.p. to delete endogenous Treg cells. Mice's weight change was monitored after
963 disease induction. (**C**) Relative body weight change after autoimmune response induction. (**D**)
964 Mice were harvested 6 days after DT injection and assessed for ki67, cytokine TNFα, IL2, and
965 IFNγ expression in $CD4^+$ cells. (**E**) Foxp3 expression among $CD4^+$ cells day 6 post DT treatment.
966 n≥5 mice per group. Data represent four independent experiments. (**F-I**) Changes relating to ion
967 balances in Te cells. (**F**) Gene sets clusters from GSEA of GO_MF and GO_Biological process
968 (GO_BP) results in $Nrn1^{-/-}$ and ctrl Te cells (Figure 4-figure supplement Table 4). (**G**) Enrichment
969 of "GOBP_ membrane repolarization" gene set and enriched gene expression heatmap. (**H**)
970 Membrane potential measurement in Te cells. Data represent two independent experiments. (**I**)
971 Enrichment of "GOMF_Metal ion transmembrane transporter activity" gene set and heatmap of
972 differential gene expression pattern (Figure 4-figure supplement 1B). (**J-N**) Metabolic changes
973 associated with $Nrn1^{-/-}$ Te cell. (**J**) Enrichment of "GOMF_amino acid transmembrane transporter
974 activity" gene set and differential gene expression heatmap. (**K**) Phosphorylation of mTOR and
975 S6 in Te cells measured by flow cytometry. n=3 replicates per group. Data represent two
976 independent experiments. (**L**) Measurement of pmTOR and pS6 in Te cells after nutrient sensing.
977 Data represent three independent experiments. (**M**) Enriched Hallmark gene sets ($p<0.05$, FDR
978 $q<0.25$). (**N**) Seahorse analysis of extracellular acidification rate (ECAR) and oxygen consumption
979 rate (OCR) in $Nrn1^{-/-}$ and ctrl Te cells. n≥6 technical replicates per group. Data represent three
980 independent experiments. Error bars indicate ±SEM. *$p<0.05$, **$p<0.01$, ***$p<0.001$,
981 ****$p<0.0001$, unpaired Student's t-test was performed for two-group comparison.
982
983
984

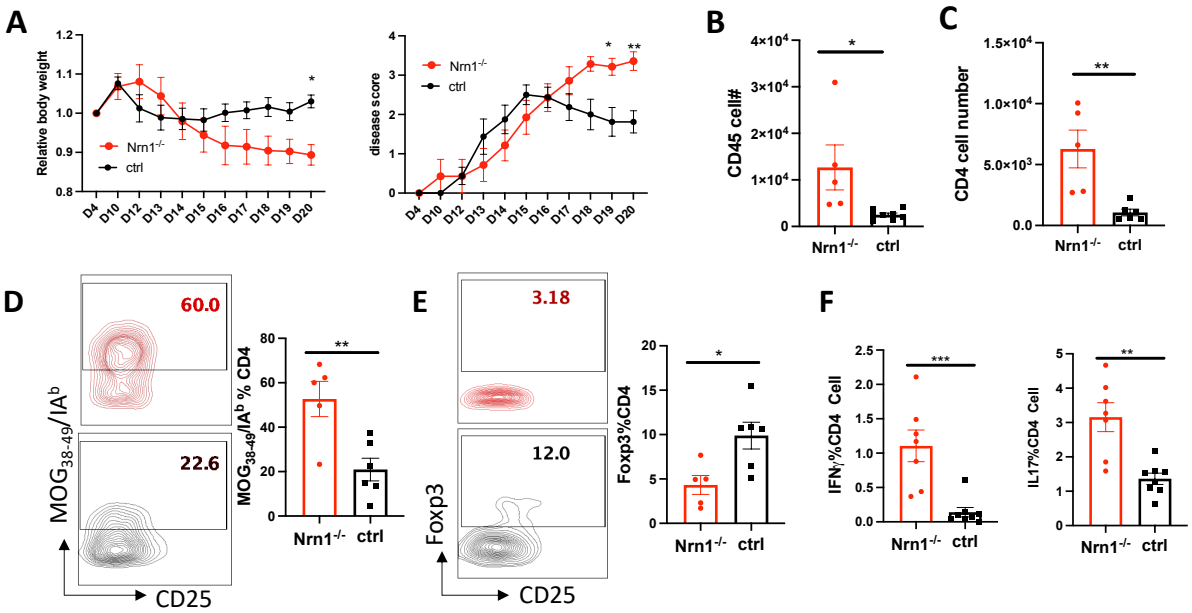

Figure 5. Nrn1 deficiency exacerbates autoimmune EAE disease.

(**A**) Aggravated body weight loss and protracted EAE disease in Nrn1$^{-/-}$ mice. (**B**) CD45^{+} cell number in the spinal cord infiltrates. (**C**) CD4^{+} cell number in the spinal cord infiltrates. (**D**) Mog$_{38-49}$/IA^{b} tetramer staining of spinal cord infiltrating CD4 cells. (**E**) Foxp3^{+} proportion among CD4^{+} cells in spinal cord infiltrates. (**F**) IFNγ^{+} and IL17^{+} cell proportion among CD4^{+} cells in draining lymph nodes. n≥5 mice per group. Data represent three independent experiments. The P value was calculated by 2way ANOVA for (**A**). The p-value was calculated by the unpaired student t-test for (**B-F**). *P<0.05, **P<0.01.